Regularization of Grad's 13-Moment-Equations in Kinetic Gas Theory

Manuel Torrilhon
Department of Mathematics &
Center for Computational Engineering Science
RWTH Aachen University
Germany
mt@mathcces.rwth-aachen.de

January 2011

Contents

Report Documentation Page

Form Approved
OMB No. 0704-0188

1. REPORT DATE	2. REPORT TYPE	3. DATES COVERED
JAN 2011	**N/A**	**-**

4. TITLE AND SUBTITLE	5a. CONTRACT NUMBER
Regularization of Grad s 13 -Moment-Equations in Kinetic Gas Theory	5b. GRANT NUMBER
	5c. PROGRAM ELEMENT NUMBER
6. AUTHOR(S)	5d. PROJECT NUMBER
	5e. TASK NUMBER
	5f. WORK UNIT NUMBER
7. PERFORMING ORGANIZATION NAME(S) AND ADDRESS(ES) **Department of Mathematics & Center for Computational Engineering Science RWTH Aachen University Germany**	8. PERFORMING ORGANIZATION REPORT NUMBER
9. SPONSORING/MONITORING AGENCY NAME(S) AND ADDRESS(ES)	10. SPONSOR/MONITOR'S ACRONYM(S)
	11. SPONSOR/MONITOR'S REPORT NUMBER(S)

12. DISTRIBUTION/AVAILABILITY STATEMENT
Approved for public release, distribution unlimited

13. SUPPLEMENTARY NOTES
See also ADA579248. Models and Computational Methods for Rarefied Flows (Modeles et methodes de calcul des coulements de gaz rarefies). RTO-EN-AVT-194

14. ABSTRACT

15. SUBJECT TERMS

16. SECURITY CLASSIFICATION OF:			17. LIMITATION OF ABSTRACT	18. NUMBER OF PAGES	19a. NAME OF RESPONSIBLE PERSON
a. REPORT **unclassified**	b. ABSTRACT **unclassified**	c. THIS PAGE **unclassified**	**SAR**	**50**	

1 Continuum Models

The accurate modeling and simulation of non-equilibrium processes in rarefied fluids or micro-flows is one of the main challenges in present fluid mechanics. The traditional models developed centuries ago are known to loose their validity in extreme physical situations. In these classical models the non-equilibrium variables, stress and heat flux, are coupled to gradients of velocity and temperature as given in the constitutive relations of Navier-Stokes and Fourier (NSF). These relations are valid close to equilibrium, however, in rarefied fluids or micro-flows the particle collisions are insufficient to maintain equilibrium. Away from equilibrium the inertia and higher order multi-scale relaxation in the fluid become dominant and essential.

1.1 Some History and Background

It is generally accepted that kinetic theory based on a statistical description of the gas provides a valid framework to describe processes in a rarefied regime or at small scales. Introductions into kinetic theory and its core, Boltzmann equation, can be found in many text books like Cercignani (1988), Cercignani (2000), Chapman and Cowling (1970) or Vincenti and Kruger (1965). The main variable used to describe the gas is the distribution function or probability density of the particle velocities which describes the number density of particles with certain velocity in each space point at a certain time. However, in many situations this detailed statistical approach yields a far too complex description of the gas. It turns out to be desirable to have a continuum model based on partial differential equations for the fluid mechanical field variables. This model should accurately approximate the multi-scale phenomena present in kinetic gas theory in a stable and compact system of field equations.

The main scaling parameter in kinetic theory is the Knudsen number Kn. It is computed from the ratio of the mean free path between collisions λ and a macroscopic length L, such that $Kn = \lambda/L$. Complete equilibrium is given for $Kn = 0$, described by the dissipationless Euler equations. In many processes gas dynamics with Navier-Stokes and Fourier fail at $Kn \approx 0.01$ and sometimes even for smaller values. Some examples will be discussed in this notes. The range of the Knudsen number is shown in Fig. 1. Similar diagrams can be found in many other texts, for example in Karniadakis and Beskok (2001). The numbers are only for orientation and may depend on the process at hand and also on the philosophy of the respective scientist. Depending on the focus of the process Navier-Stokes-Fourier can be used up to a Knudsen number between 10^{-2} and 10^{-1}. On the other hand, for large Knudsen numbers the collisions between the particles can be neglected and they move ballistically in a free flight.

The range between these limiting cases can be split into two parts. One part is the kinetic regime in which the non-equilibrium is so strong that a detailed description by a distribution function becomes necessary. In this regime either the Boltzmann equation is solved directly or the direct simulation Monte-Carlo (DSMC) method is employed, see Bird (1998). The other part is the so-called transition regime where a fluid description is still possible, although a larger set of field variables and/or higher derivatives may be needed. In this regime Boltzmann simulations or DSMC become increasingly expensive. The limit for the continuum models is currently around $Kn = 1$, depending on the process.

The aim of the research is to establish continuum models and to push their limit further. The transition regime is typically split further into a slip regime at lower Knudsen number. However, we will see below that with the relevance of slip also bulk effects occur that can not be described by advanced boundary modeling only.

There exist two classical approaches to the transition regime. Close to the limit $Kn \to 0$ an asymptotic analysis in powers of the Knudsen number, called Chapman-Enskog expansion, leads in first order to the classical NSF relations including specific expressions of the transport coefficients, see the textbook Chapman and Cowling (1970). The Chapman-Enskog expansion can be used to derive higher order constitutive relations from the Boltzmann equation. The resulting equations are called Burnett equations for the second order and super-Burnett in case of third order. They include ever higher gradients of temperature and velocity into the constitutive relations for stress and heat flux. The relations of super-Burnett order for the full Boltzmann equation are already forbiddingly complex and even higher order was never considered. Furthermore, in general the corrections of higher than first order, i.e., Burnett and super-Burnett relations, are known to be unstable, as shown by Bobylev (1982). In special cases the Burnett equations have been used to calculate higher Knudsen number flow, for example by Agarwal et al. (2001), Lockerby and Reese (2003), or Xu and Li (2004). In some cases the instability of Burnett equations could be overcome by ad-hoc modifications as in Zhong et al. (1993) or in Xu (2002). However, general stable Burnett relations that follow rigorously from the Boltzmann equation seem not to exist.

An alternative approximation strategy in kinetic theory is given by Grad's moment method based on Hilbert expansion of the distribution function in Hermite polynomials. The method is described in Grad (1949) and Grad (1958). In contrast to Chapman-Enskog and Burnett this method extends the set of variables of a possible continuum model beyond the fields of density, velocity and temperature. The additional variables are given by higher moments of the distribution function. The 13-moment-case of Grad considers evolution equations for density, velocity and temperature *and* stress tensor and heat flux. Higher moment theories include more moments which lack physical intuition. In the context of phenomenological thermodynamics extended theories proved to be successful in many test cases, see the text book Müller and Ruggeri (1998) or, e.g., Jou et al. (1996). Both approaches, Chapman-Enskog and Grad, are explained in detail elsewhere in this book.

Large moment systems based on Grad's approach with hundreds of variables where used to describe shock structures, see the dissertation of Au (2001), the shock-tube experiment in the work Au et al. (2001), and heat conduction in Struchtrup (2002). A computationally efficient approach to large moment systems is using comulant theory, see Seeger and Hoffmann (2000). However, even though the capability of Grad's moment method is assured by these results, its usefulness is restricted due to slow convergence. Indeed, many moments are needed to describe high non-equilibrium which results in large systems of partial differential equations to be solved.

Moment systems provide a rich mathematical structure like hyperbolicity and entropy law discussed, e.g., in Müller and Ruggeri (1998) and in Levermore (1996). It has been argued that evolution equations in physics should always be hyperbolic in order to provide a finite speed of propagation. When using a nonlinear extension of Grad's approach based on the maximum-entropy-principle as in Müller and Ruggeri (1998) and Levermore (1996),

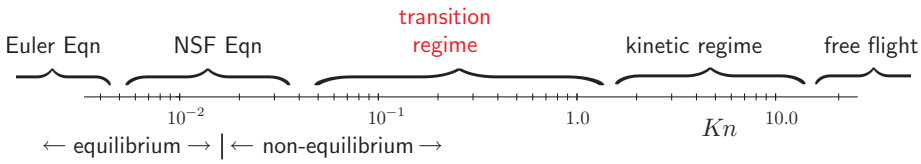

Figure 1: Overview of the range of Knudsen number and various model regimes.

the moment systems lead to stable hyperbolic equations. However, in practical explicit systems hyperbolicity is given only in a finite range due to linearization. In Junk (1998) and Junk (2002) it is shown that the fully nonlinear maximum-entropy approach has sever drawbacks and singularities. Furthermore, the hyperbolicity leads to discontinuous sub-shock solutions in the shock profile. A variant of the moment method has been proposed by Eu (1980) and is used, e.g., in Myong (2001). Recently, a maximum-entropy 10-moment system has been used by Suzuki and van Leer (2005).

Both fundamental approaches of kinetic theory, Chapman-Enskog and Grad, exhibit severe disadvantages. Higher order Chapman-Enskog expansions are unstable and Grad's method introduces subshocks and show slow convergence. It seems to be desirable to combine both methods in order to remedy their disadvantages. Such an hybrid approach have already been discussed by Grad in a side note in Grad (1958). He derives a variant of the regularized 13-moment equations given below, but surprisingly he neither gives any details nor is he using or investigating the equations. In the last fifty years the paper Grad (1958) was cited as standard source for introduction into kinetic theory, but, apparently, this specific idea got entirely lost and seems not to be known in present day literature.

The Chapman-Enskog expansion is based on equilibrium and the corrections describe the non-equilibrium perturbation. A hybrid version which uses a non-equilibrium as basis is discussed in Karlin et al. (1998). They deduced linearized equations with unspecified coefficients. Starting from Burnett equations Jin and Slemrod (2001) derived an extended system of evolution equations which resembles the regularized 13-moment system. It is solved numerically in Jin et al. (2002). However, the tensorial structure of their relations is not in accordance with Boltzmann's equation. Starting from higher moment systems Müller et al. (2003) discussed a parabolization which includes higher order expressions into hyperbolic equations.

The regularized 13-moment-equations presented below were rigorously derived from Boltzmann's equation in Struchtrup and Torrilhon (2003). The key ingredient is a Chapman-Enskog expansion around a pseudo-equilibrium which is given by the constitutive relations of Grad for stress tensor and heat flux. The final system consists of evolution equations for the fluid fields: density, velocity, temperature, stress tensor and heat flux. The closure procedure adds second order derivatives to Grad's evolution equations of stress and heat flux, thus regularizes the former hyperbolic equations into a mixed hyperbolic-parabolic system with relaxation. The relaxational and parabolic part is only present in the equations of stress and heat flux and models the multi-scale dissipation of Boltzmann's equation, see Struchtrup and Torrilhon (2003). Like the Boltzmann equation the R13 system is derived for monatomic gases and all the results in this chapter are restricted to this case. The extension to poly-atomic gases or mixtures is future work. The text book by Struchtrup (2005b) provides an introduction to approximation methods in kinetic theory

including the regularized moment equations. However, recent developments on boundary conditions and boundary value problems are not covered.

1.2 Added Value of Continuum Equations

Predictive simulations of non-equilibrium flows of gases in rarefied regimes of micro-scale situations are important for many technical applications. Direct solutions of Boltzmann's equation or the stochastic particle method (DSMC) give very accurate results in principle for the whole range of the Knudsen number. However, computational expense remains a major drawback and is considered as an important argument for the use of continuum models in the transition regime. However, there is another interesting fact that is often underestimated. Non-equilibrium flows exhibit behavior which is in contrast to the intuition of fluid dynamics and difficult to understand. The simulations of Boltzmann and DSMC may give accurate predictions of this behavior but it is important to realize that their results actually do not easily provide a detailed *physical understanding* of the process.

The reason is that our understanding of physical phenomena is very often based on the structure and qualitative behavior of differential equations and their solutions. Many aspect of fluid dynamics like convection, viscosity, heat conduction are closely linked to particular aspects of the differential equations describing the flow. Our understanding of these phenomena arise from analytical solutions for small models that display how the coupling of the mathematical terms influence the behavior of the solution, which is then directly (and sometimes too quickly) translated into reality.

The mere simulation result of Boltzmann or DSMC does not allow this kind of understanding. Effects and phenomena in the solution are hard or impossible to trace back to certain aspects of the model. There are many simple questions these simulation techniques can not answer. DSMC for example always solves for the full non-linear situation and the question what is a linear effect can not be answered. Similarly, it is impossible to produce isothermal results or switching off heat conductivity in both Boltzmann and DSMC computations.

The underestimated added value of continuum equations is that ideally they come with manageable partial differential equations which allow to identify physical effects and coupling phenomena that occur in non-equilibrium flows. Analytical solutions for model situations provide physical insight into the intriguing flow patterns and helps to understand rarefaction effects. This particular aspect of a continuum model like the R13-equations goes beyond any kinetic simulation result.

2 Regularized 13-Moment-Equations

Here, we will present the fully nonlinear R13 equations and their background. An overview of the derivation is given, but for the details Struchtrup and Torrilhon (2003) and Struchtrup (2005b) should be consulted. We assume the reader is familiar with Chapman-Enskog expansion and Grad's moment method.

2.1 Kinetic Gas Theory

Starting point for the regularized 13-moment-equations is kinetic gas theory (see Cercignani (1988)) where we denote the distribution function by $f(\mathbf{x}, t, \mathbf{c})$ describing the probability density to find a particle at space point $\mathbf{x}$ and time t with velocity $\mathbf{c}$. The distribution function is governed by the Boltzmann equation

$$\frac{\partial f}{\partial t} + c_i \frac{\partial f}{\partial x_i} = S(f, f) \tag{1}$$

first presented in Boltzmann (1872). Here we neglect external forces and abbreviate the collision integral by $S(f, f)$. Originating from kinetic gas theory all variables of the R13 equations are based on moments of $f(\mathbf{x}, t, \mathbf{c})$. The mass density

$$\rho(\mathbf{x}, t) = m \int_{\mathbb{R}^3} f(\mathbf{x}, t, \mathbf{c})\, d\mathbf{c} \tag{2}$$

as well as the velocity and internal energy

$$v_i(\mathbf{x}, t) = \frac{m}{\rho(\mathbf{x}, t)} \int_{\mathbb{R}^3} c_i\, f(\mathbf{x}, t, \mathbf{c})\, d\mathbf{c}, \quad \varepsilon(\mathbf{x}, t) = \frac{m}{\rho(\mathbf{x}, t)} \int_{\mathbb{R}^3} \frac{1}{2} (c_i - v_i)^2\, f(\mathbf{x}, t, \mathbf{c})\, d\mathbf{c} \tag{3}$$

form the basic equilibrium variables of the gas. The mass of the particles is given by m. The pressure is given by $p = \frac{2}{3}\rho\varepsilon$ due to the assumption of monatomic gases and we will use the temperature $\theta = \frac{k}{m}T$ in energy units, i.e., $p = \rho\theta$. The R13 system describes the state of the gas by including the first two non-equilibrium variables, stress tensor and heat flux,

$$\sigma_{ij}(\mathbf{x}, t) = m \int_{\mathbb{R}^3} C_{<i} C_{j>}\, f(\mathbf{x}, t, \mathbf{C})\, d\mathbf{C}, \quad q_i(\mathbf{x}, t) = m \int_{\mathbb{R}^3} \frac{1}{2} C_i C^2\, f(\mathbf{x}, t, \mathbf{C})\, d\mathbf{C} \tag{4}$$

which are based on the microscopic peculiar velocity $C_i = c_i - v_i$. In total we have 13 three dimensional fields and the R13 equations are evolution equations for (2)-(4).

We will mostly use indexed quantities to describe vectors and tensors and summation convention for operations between them. Bold letters will be used in occasional invariant formulations. The Kronecker symbol δ_{ij} denotes the identity matrix $\mathbf{I}$. Angular brackets denote the deviatoric (trace-free) and symmetric part of a tensor, i.e., $A_{\langle ij \rangle} = \frac{1}{2}(A_{ij} + A_{ji}) - \frac{1}{3}A_{kk}\delta_{ij}$. Beside the angular brackets normal brackets are used to abbreviate the normalized sum of index-permutated tensor expressions, i.e., $A_{(ij)} = \frac{1}{2}(A_{ij} + A_{ji})$. An introduction to tensorial operations also on higher order tensors can be find in Struchtrup (2005b).

The stress tensor is related to the pressure tensor p_{ij} by $p_{ij} = p\delta_{ij} + \sigma_{ij}$, which will be used frequently. The temperature tensor can be computed from the definition $\Theta_{ij} = p_{ij}/\rho = \theta\delta_{ij} + \sigma_{ij}/\rho$. This tensor satisfies $\Theta_{kk} = 3\theta$. The diagonal entries of the pressure and temperature tensor are sometimes referred to as directional pressures or multiple temperatures, like in Candler et al. (1994). If the temperature tensor is scaled by $\hat{\Theta}_{ij} = \Theta_{ij}/\theta$ each diagonal entry and the trace lies between the values 0 and 3. In equilibrium all scaled directional temperatures reduce to unity.

2.2 Derivation

The derivation of the regularized 13-moment-equations has been done in two ways. Both ways give specific insight into the structure and properties of the theory. Here, we only give a very general overview of the derivation.

2.2.1 Based on a Pseudo-Time-Scale

The original derivation Struchtrup and Torrilhon (2003) develops an enhanced constitutive theory for Grad's moment equations. The closure procedure of Grad is too rigid and needs to be relaxed. The new theory can be summarized in three steps

1) Identify the set of variables U and higher moments V that need a constitutive relation in Grad's theory.

2) Formulate evolution equations for the difference $R = V - V^{(\mathrm{Grad})}(U)$ of the constitutive moments and their Grad relation.

3) Perform an asymptotic expansion of R alone while fixing *all* variables U of Grad's theory.

This procedure can in principle be performed on any system obtained by Grad's moment method, i.e., any number of moments can be considered as basic set of variables. For the derivation of R13 the first 13 moments density, velocity, temperature, stress deviator and heat flux have been considered in accordance with the classical 13-moment-case of Grad.

In the classical Grad approach the difference R is considered to be zero: All constitutive moments follow from lower moments by means of Grad's distribution $V = V^{(\mathrm{Grad})}(U)$. This rigidity causes hyperbolicity but also artifacts like subshocks and poor accuracy. However, the evolution equation for R is in general not an identity. Instead it describes possible deviations of Grad's closure. The constitutive theory of R13 takes these deviations into account.

The evolution equation for R can not be solved exactly because it is influenced by even higher moments. Hence, an approximation is found by asymptotic expansion. In doing this, step 3 requires a modeling assumption about a scaling cascade of the higher order moments. In the asymptotic expansion of R we fix lower moments, that is, density, velocity and temperature, but also non-equilibrium quantities like stress and heat flux. The assumption is a pseudo-time-scale such that the higher moments R follow a faster relaxation. The expansion can also be considered as an expansion around a non-equilibrium (pseudo-equilibrium). A similar idea has been formulated in Karlin et al. (1998) based solely on distribution functions.

The result for R after one expansion step is a relation that couples R to gradients of the variables U, in R13 these are gradients of stress and heat flux. The gradient terms enter the divergences in the equations for stress and heat flux and produce dissipative second order derivatives. The final system is a regularization of Grad's 13-moment-equations. The procedure resembles the derivation of the NSF-system. Indeed the NSF equations can be considered as regularization of Euler equations (i.e., Grad's 5-moment-system).

2.2.2 Based on Order of Magnitude

The Order-of-Magnitude-Method presented in Struchtrup (2004, 2005a) considers the infinite system of moment equations resulting from Boltzmann's equation. It does not depend on Grad's closure relations and does not directly utilize the result of asymptotic expansions. The method finds the proper equations with order of accuracy λ_0 in the Knudsen number by the following three steps:

1) Determination of the order of magnitude λ of the moments.

2) Construction of moment set with minimum number of moments at order λ.

3) Deletion of all terms in all equations that would lead only to contributions of orders $\lambda > \lambda_0$ in the conservation laws for energy and momentum.

Step 1 is based on a Chapman-Enskog expansion where a moment φ is expanded according to $\varphi = \varphi_0 + Kn\,\varphi_1 + Kn^2\varphi_2 + ...$, and the leading order of φ is determined by inserting this ansatz into the complete set of moment equations. A moment is said to be of leading order λ if $\varphi_\beta = 0$ for all $\beta < \lambda$. This first step agrees with the ideas of Müller et al. (2003). Alternatively, the order of magnitude of the moments can be found from the principle that a single term in an equation cannot be larger in size by one or several orders of magnitude than all other terms.

In Step 2, new variables are introduced by linear combination of the moments originally chosen. The new variables are constructed such that the number of moments at a given order λ is minimal. This step gives an unambiguous set of moments at order λ.

Step 3 follows from the definition of the order of accuracy λ_0: A set of equations is said to be accurate of order λ_0, when stress and heat flux are known within the order $\mathcal{O}\left(Kn^{\lambda_0}\right)$.

The order of magnitude method gives the Euler and NSF equations at zeroth and first order, and thus agrees with the Chapman-Enskog method in the lower orders, seeStruchtrup (2004). The second order equations turn out to be Grad's 13 moment equations for Maxwell molecules as shown in Struchtrup (2004), and a generalization of these for molecules that interact with power potentials, see Struchtrup (2005a). At third order, the method was only performed for Maxwell molecules, where it yields the R13 equations in Struchtrup (2004). It follows that R13 satisfies some optimality when processes are to be described with third order accuracy. In all these cases the method has been performed on the moments and their transfer equations. For linear kinetic equations the method has been generalized to the kinetic description in Kauf et al. (2010) and it is precisely shown how the approximation of the distribution function is implied by the kinetic equation itself.

Note that the derivation based on pseudo-time-scales above requires an unphysical assumption, namely strongly different relaxation times for different moments. Such a cascading does not exist since all moments relax on roughly the same time scale proportional to Kn. The order-of-magnitude approach does not rely on such an assumption. Instead of different relaxation times this method induces a structure on the set of non-equilibrium moments based on size, that is, order of magnitude and justifies different closed systems of moment equations.

2.3 Evolution equations

The evolution equations for density, velocity and internal energy are given by the conservation laws of mass, momentum and energy,

$$\frac{D\rho}{Dt} + \rho\frac{\partial v_k}{\partial x_k} = 0 \tag{5}$$

$$\rho\frac{Dv_i}{Dt} + \frac{\partial p}{\partial x_i} + \frac{\partial \sigma_{ij}}{\partial x_j} = 0 \tag{6}$$

$$\rho\frac{D\varepsilon}{Dt} + p\frac{\partial v_i}{\partial x_i} + \sigma_{ij}\frac{\partial v_i}{\partial x_j} + \frac{\partial q_i}{\partial x_i} = 0 \tag{7}$$

including the stress tensor σ_{ij} and the heat flux q_i. The R13 equations can be viewed as a generalized constitutive theory for stress tensor and heat flux. The standard local relations of Navier-Stokes and Fourier are extended to form full evolution equations for σ_{ij} and q_i. They are given by

$$\frac{\partial \sigma_{ij}}{\partial t} + \frac{\partial \sigma_{ij} v_k}{\partial x_k} + \frac{4}{5}\frac{\partial q_{\langle i}}{\partial x_{j\rangle}} + 2p\frac{\partial v_{\langle i}}{\partial x_{j\rangle}} + 2\sigma_{k\langle i}\frac{\partial v_{j\rangle}}{\partial x_k} + \frac{\partial m_{ijk}}{\partial x_k} = -\nu\,\sigma_{ij} \tag{8}$$

for the stress, and

$$\frac{\partial q_i}{\partial t} + \frac{\partial q_i v_k}{\partial x_k} + q_k\frac{\partial v_i}{\partial x_k} - \left(\frac{5}{2}p\,\delta_{ij} + \sigma_{ij}\right)\frac{1}{\rho}\frac{\partial \sigma_{jk}}{\partial x_k} - \sigma_{ij}\frac{1}{\rho}\frac{\partial p}{\partial x_j} + \frac{5}{2}p\frac{\partial \theta}{\partial x_i} + \left(\frac{6}{5}\delta_{(ij}q_{k)} + m_{ijk}\right)\frac{\partial v_j}{\partial x_k} + \frac{1}{2}\frac{\partial \bar{R}_{ik}}{\partial x_k} = -\nu\frac{2}{3}q_i \tag{9}$$

for the heat flux where we used the abbreviation

$$\bar{R}_{ij} = 7\theta\sigma_{ij} + R_{ij} + \frac{1}{3}R\delta_{ij}. \tag{10}$$

Both equations form quasi-linear first order equations with relaxation. The inverse relaxation time is given proportional to ν, which is the local mean collision frequency of the gas particles to be specified below.

The remaining unspecified quantities are m_{ijk}, R_{ij} and R. They represent higher moments and stem from higher moments contributions in the transfer equations of Boltzmann's equation. Neglecting these expressions turns the system (5)-(9) into the classical 13-moment-case of Grad (1949) and Grad (1958). In Struchtrup and Torrilhon (2003) gradient expressions are derived for m_{ijk}, R_{ij} and R which regularize Grad's equations and turn them into a highly accurate non-equilibrium flow model. The R13 theory provides the gradient expressions

$$\begin{aligned} m_{ijk} &= -2\frac{p}{\nu}\frac{\partial(\sigma_{\langle ij}/\rho)}{\partial x_{k\rangle}} + \frac{8}{10p}q_{\langle i}\sigma^{(1)}_{jk\rangle}\,, \\ R_{ij} &= -\frac{24}{5}\frac{p}{\nu}\frac{\partial(q_{\langle j}/\rho)}{\partial x_{j\rangle}} + \frac{32}{25p}q_{\langle i}q^{(1)}_{j\rangle} + \frac{24}{7\rho}\sigma_{k\langle i}\sigma^{(1)}_{j\rangle k}\,, \\ R &= -12\frac{p}{\nu}\frac{\partial(q_k/\rho)}{\partial x_k} + \frac{8}{p}q_k q^{(1)}_k + \frac{6}{\rho}\sigma_{ij}\sigma^{(1)}_{ij}\,. \end{aligned} \tag{11}$$

with the abbreviations

$$\sigma_{ij}^{(1)} = -2\frac{p}{\nu}\,\frac{\partial v_{\langle i}}{\partial x_{j\rangle}}, \qquad q_i^{(1)} = -\frac{15}{4}\frac{p}{\nu}\,\frac{\partial \theta}{\partial x_i}. \tag{12}$$

The relations (11) with (8) and (9) complete the conservation laws (5)-(7) to form the system of regularized 13-moment-equations.

The evolution equations above are not in balance law form. Usually, the constitutive theory is more easily based directly on these primitive or internal variables. However, since the equations originated from transfer equations in balance law form, such a formulation can be found. We have

$$\frac{\partial}{\partial t}\rho + \frac{\partial}{\partial x_k}(\varrho v_k) = 0 \tag{13}$$

$$\frac{\partial}{\partial t}(\rho v_i) + \frac{\partial}{\partial x_k}\left(\rho v_i v_k + p_{ik}\right) = 0 \tag{14}$$

$$\frac{\partial}{\partial t}\left(p_{ij} + \rho v_i v_j\right) + \frac{\partial}{\partial x_k}\left(\rho v_i v_j v_k + 3p_{(ij}v_{k)} + M_{ijk}\right) = -\nu\,\sigma_{ij} \tag{15}$$

$$\partial_t Q_i + \partial_j\left(2Q_{(i}v_{j)} - E\,v_i v_j + M_{ijk}v_k + \tfrac{1}{2}\left(p_{ij}v_k^2 + 5\theta p\delta_{ij} + \bar{R}_{ij}\right)\right) = -\nu(\sigma_{ij}v_j + \tfrac{2}{3}q_i) \tag{16}$$

as R13 system equivalent to (5)-(9). Here, the evolved quantities are the so-called convective moments. In this formulation it turned out to be more natural to use the pressure tensor p_{ij} as variable. Hence, the energy equation and the equation for the stress tensor are merged into a single row in (13). The energy equation may be recovered by taking the trace of this row. The equation for the heat flux is written as an equation for the total energy flux $Q_i = E\,v_i + p_{ik}v_k + q_i$ with total energy $E = \frac{1}{2}\rho v_j^2 + \frac{3}{2}p$. Additionally, the abbreviation $M_{ijk} = \frac{6}{5}\delta_{(ij}q_{k)} + m_{ijk}$ is used.

The system (13)-(16) has the form

$$\partial_t U + \operatorname{div}\mathbf{F}(U) = P(U) \tag{17}$$

with a flux function $\mathbf{F}$ and a relaxational source P. In the regularized case $\mathbf{F}$ contains diffusive gradient terms. The convective variables are given by

$$U = \{\rho, \rho v_i, p_{ij} + \rho v_i v_j, E\,v_i + p_{ik}v_k + q_i\} \tag{18}$$

and the flux function may be split into the three directions and four convective variables

$$\mathbf{F}(U) = \begin{pmatrix} F^{(\rho),x} & F^{(\rho),y} & F^{(\rho),z} \\ F_i^{(v),x} & F_i^{(v),y} & F_i^{(v),z} \\ F_{ij}^{(P),x} & F_{ij}^{(P),y} & F_{ij}^{(P),z} \\ F_i^{(Q),x} & F_i^{(Q),y} & F_i^{(Q),z} \end{pmatrix}. \tag{19}$$

2.4 Stability and Asymptotic Accuracy

We will briefly discuss the asymptotics of the R13 system, especially the relation to classical hydrodynamics, as well as commenting on the stability of the system. Most of this discussion was done in detail in Struchtrup and Torrilhon (2003) and Torrilhon and Struchtrup (2004) based on asymptotic analysis and linear stability theory.

The mean collision frequency is given by ν and appears at the right hand side of the R13 equations. Introducing the mean free path at a reference state by

$$\lambda_0 = \frac{\sqrt{\theta_0}}{\nu_0} \tag{20}$$

we have the fundamental microscopic length scale. Macroscopic length and time scales are fixed such that

$$x_0/t_0 = \sqrt{\theta_0} \tag{21}$$

where $\sqrt{\theta_0}$ represents the isothermal equilibrium speed of sound. It is considered as the velocity scale in the system. Note that all moments can be scaled by a reference density ρ_0 and appropriate powers of $\sqrt{\theta_0}$. The Knudsen number is defined by

$$Kn = \frac{\lambda_0}{x_0} = \frac{1}{\nu_0 t_0} \tag{22}$$

and appears as factor $1/Kn$ at the right hand side of the dimensionless equations. In applications close to equilibrium the Knudsen number is a small number $Kn < 1$. Hence, an asymptotic expansion in powers of Kn is reasonable. In the spirit of a Chapman-Enskog-expansion we write down

$$\sigma_{ij} = \sigma_{ij}^{(0)} + Kn\,\sigma_{ij}^{(1)} + Kn^2\,\sigma_{ij}^{(2)} + \ldots \tag{23}$$

$$q_i = q_i^{(0)} + Kn\,q_i^{(1)} + Kn^2\,q_i^{(2)} + \ldots \tag{24}$$

for the stress tensor and heat flux. This expansion can now be introduced into the full Boltzmann equation, see Chapman and Cowling (1970), Vincenti and Kruger (1965), or in any continuum model, like the R13 system (5)-(11). In general, the result will differ at a certain stage of the expansion.

Assuming the validity of Boltzmann's equation, we define the difference in asymptotic expansions as a measure for the accuracy of the continuum model.

Definition 1 (Knudsen order) *Assume the macroscopic fields $U^{(Boltz)}$ and $U^{(Model)}$ are the respective solutions for Boltzmann's equations and a continuum model. If, after asymptotic expansion in the Knudsen number Kn, the stress tensor and heat flux satisfy in some appropriate norm*

$$\left\|\boldsymbol{\sigma}^{(Model)} - \boldsymbol{\sigma}^{(Boltz)}\right\| + \left\|\mathbf{q}^{(Model)} - \mathbf{q}^{(Boltz)}\right\| = \mathcal{O}\left(Kn^{n+1}\right),$$

the accuracy or Knudsen order of the model is $n \in \mathbb{N}$.

According to this definition a system with Knudsen order n have n coefficients in their asymptotic expansion for σ_{ij} and q_i matching with those of the Chapman-Enskog expansion of the Boltzmann equation. It is well known that the laws of Navier-Stokes and Fourier match the first (linear) coefficient of the Chapman-Enskog expansion and thus, the NSF system exhibits Knudsen order $n = 1$. Consequently, the non-dissipative Euler equations have $n = 0$, while it turns out that Grad's equations have $n = 2$, at least when considering an interaction potential of Maxwell type, see Struchtrup (2005b). Also, the

Burnett equations which use the next contribution of the Chapman-Enskog expansion have $n = 2$, by definition.

In Torrilhon and Struchtrup (2004) it was shown that Chapman-Enskog expansion of the R13 system leads to the result of Boltzmann's equation *up to third order in* Kn at least for the case of Maxwell molecules.

Theorem 1 (R13 Stability and Accuracy) *The non-linear regularized 13-moment equations for Maxwell molecules exhibit a Knudsen order*

$$n\,(R13) = 3,$$

hence, they are of super-Burnett order.

The result is true for the full nonlinear and three-dimensional system with linear temperature-dependence of viscosity, according to Maxwell molecules. This means that any R13 result will asymptotically differ from a full Boltzmann simulation for Maxwell molecules only with an error in $\mathcal{O}\,(Kn^4)$. For other interaction potentials the Knudsen order formally reduces but only for the nonlinear equations.

The first order of the expansion gives the relations of Navier-Stokes and Fourier of compressible gas dynamics for both the Boltzmann equation and the R13 system. The expressions are given by

$$\sigma_{ij}^{(1)} = -2\frac{p}{\nu}\frac{\partial v_{\langle i}}{\partial x_{j\rangle}} \quad \text{and} \quad q_i^{(1)} = -\frac{15}{4}\frac{p}{\nu}\frac{\partial \theta}{\partial x_i}. \tag{25}$$

This shows that for very small Knudsen numbers the R13 system will essentially behave like the NSF equations. From (25) we can identify the transport coefficients and relate them to the mean collision frequency in order to have a practical expression for ν. Usually the viscosity is given by

$$\mu\,(\theta) = \mu_0 \left(\frac{\theta}{\theta_0}\right)^s \tag{26}$$

with a temperature exponent $0.5 \leq s \leq 1$. Hence, we will use

$$\nu\,(\theta) = \frac{p}{\mu\,(\theta)} = \rho\,\theta^{1-s}\frac{\theta_0^s}{\mu_0} \tag{27}$$

for the collision frequency which leads to asymptotically correct transport coefficients. Sometimes it is asked what the transport coefficients are used in the R13 system. However, the term "transport coefficients", i.e., coefficients in (25), is not defined for the system, since the relations (25) are entirely substituted by the evolution equations (8) and (9). The definition of the collision frequency leads to the expression

$$\lambda_0 = \frac{\mu_0}{\rho_0\sqrt{\theta_0}} \tag{28}$$

for the mean free path. This differs from a standard value

$$\bar{\lambda}_0 = \frac{4}{5}\frac{\mu_0}{\rho_0\sqrt{\frac{\pi}{8}\theta_0}} \tag{29}$$

given e.g., in Chapman and Cowling (1970), by a factor of $\frac{4}{5}\sqrt{\frac{8}{\pi}} \approx 1.28$. The definition (20) is used to avoid additional factors in the dimensionless equations.

In Torrilhon and Struchtrup (2004) also the stability of the R13 system was studied based on linear wave of the form $\phi(x,t) = \hat{\phi}\exp(\mathbf{i}(\omega(k)t - kx))$. For stability wave modes with wave number k need to be damped in time, such that $\operatorname{Im}\omega(k) > 0$ is necessary. It is well known that the Burnett equations fail on this requirement, see Bobylev (1982). They exhibit modes which become unstable for small wave lengths. On the contrary, the R13 shows full stability.

Theorem 2 (R13 Stability) *When considering small amplitude linear waves, the R13 system is linearly stable in time for all modes and wave lengths.*

The instability of the Burnett system indicates problems with the unreflected usage of the Chapman-Enskog expansion. However, the NSF system is stable, hence the expansion technique must not be completely abandoned. There is reason to believe that the first expansion steps is more robust over the higher order contribution. In particular, R13 uses one expansion step and exhibits stability. However, for some collision models, namely BGK relaxation, also the Burnett equations show linear stability. A clear statement about the quality of the failure of the Chapman-Enskog expansion is not available.

Fig. 2 shows the damping factor of the different modes in NSF, Burnett, Grad and R13 theory. NSF and Burnett have three modes, while Grad and R13 have five (one trivial mode is suppressed in the plot). Unstable negative damping is marked as grey region in the plots and the failure of Burnett is clearly seen.

With these properties the R13 system is formally the most accurate stable continuum model currently available.

2.5 Explicit 2D equations

In two dimensions the set of variables reduce and we consider the reduced set in the notation

$$v_i = (v_x, v_y, 0)\,, \quad p_{ij} = \begin{pmatrix} p_x & p_{xy} & 0 \\ p_{xy} & p_y & 0 \\ 0 & 0 & p_z \end{pmatrix}, \quad q_i = (q_x, q_y, 0) \tag{30}$$

assuming homogeneity in the z-direction. We denote the directional pressures by p_x, p_y, and p_z. Note, that while the shear stresses p_{xz} and p_{yz} vanish the diagonal element p_z might be different from zero. This follows from the kinetic definition of $p_z = \int C_z^2 f\, d\mathbf{C}$. In z-direction the distribution function is assumed to be isotropic, but it may deviate isotropically from its equilibrium value. Hence, all even moments such as p_z will have a non-equilibrium value.

Instead of the directional pressures p_x, p_y and p_z we will consider p_x, p_y and the full pressure $p = \frac{1}{3}(p_x + p_y + p_z)$ as basic variables. The single shear stress will be denoted by $\sigma := \sigma_{xy} = p_{xy}$. Together with the density we have 9 independent variables for the two-dimensional R13 equations given by

$$W = \{\rho, v_x, v_y, p, p_x, p_y, \sigma, q_x, q_y\}\,. \tag{31}$$

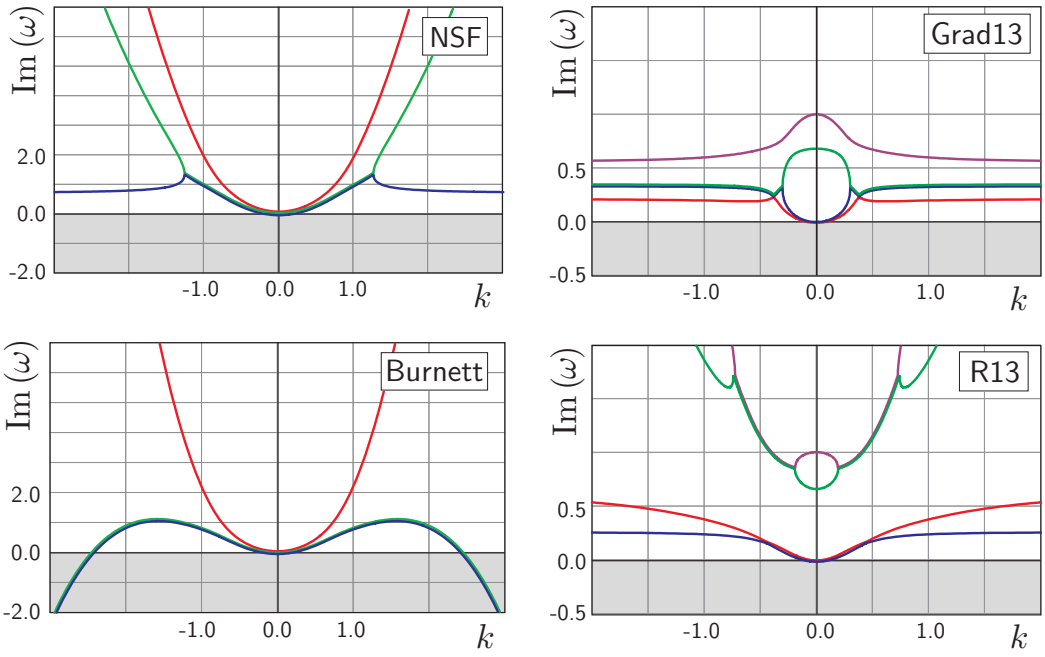

Figure 2: Damping coefficients of various models. The grey region marks the unstable regime.

In the following the abbreviation $v^2 = v_x^2 + v_y^2$ for the square of the velocity vector is used. Note that, in one-dimensional calculations the set of variables is further reduced. We have $v_y = q_y = p_{xy} = 0$ and $p_y = p_z$, hence 5 variables $\{\rho, v_x, p, p_x, q_x\}$ remain. Consider the full 2d variable set but restrict the spatial dependence to one dimension is sometimes called 1.5 dimensional.

As shown above the equations can be written in the balance law form

$$\partial_t U(W) + \operatorname{div} \mathbf{F}(W) = P(W). \tag{32}$$

Here, the two-dimensional divergence $\operatorname{div} = (\partial_x, \partial_y)$ is used and the flux function is split into $\mathbf{F}(W) = (F(W), G(W))$. Since the tensorial notation in (13)-(16) does not provide an easy detailed insight into the explicit equations we proceed with giving explicit functions for U, F, G and P written in the variables (31). For better readability we split $U = (U_1, U_2)$ and write

$$U_1(W) = \begin{pmatrix} \rho \\ \rho v_x \\ \rho v_y \\ \frac{1}{2}\rho v^2 + \frac{3}{2}p \end{pmatrix}, \quad U_2(W) = \begin{pmatrix} \rho v_x^2 + p_x \\ \rho v_y^2 + p_y \\ \rho v_x v_y + \sigma \\ E v_x + p_x v_x + \sigma v_y + q_x \\ E v_y + p_y v_y + \sigma v_x + q_y \end{pmatrix} \tag{33}$$

where we again used the total energy $E = \frac{1}{2}\rho v^2 + \frac{3}{2}p$. Using the total energy flux

$$Q_x = E v_x + p_x v_x + \sigma v_y + q_x \tag{34}$$
$$Q_y = E v_y + \sigma v_x + p_y v_y + q_y \tag{35}$$

the flux functions are written

$$F(W) = \begin{pmatrix} \rho v_x \\ \rho v_x^2 + p_x \\ \rho v_x v_y + \sigma \\ E v_x + p_x v_x + \sigma v_y + q_x \\ \rho v_x^3 + 3 p_x v_x + \frac{6}{5} q_x + m_{xxx} \\ \rho v_x v_y^2 + p_y v_x + 2\sigma v_y + \frac{2}{5} q_x + m_{xyy} \\ \rho v_y v_x^2 + p_x v_y + 2\sigma v_x + \frac{2}{5} q_y + m_{xxy} \\ 2 Q_x v_x - E v_x^2 + M_{xxx} v_x + M_{xxy} v_y + \frac{1}{2}\left(p_x v^2 + \bar{R}_{xx}\right) \\ Q_x v_y + Q_y v_x - E v_x v_y + M_{xxy} v_x + M_{xyy} v_y + \frac{1}{2}\left(\sigma v^2 + \bar{R}_{xy}\right) \end{pmatrix} \tag{36}$$

for the x-direction and

$$G(W) = \begin{pmatrix} \rho v_y \\ \rho v_x v_y + \sigma \\ \rho v_y^2 + p_y \\ E v_y + p_y v_y + \sigma v_x + q_y \\ \rho v_y v_x^2 + p_x v_y + 2\sigma v_x + \frac{2}{5} q_x + m_{yxx} \\ \rho v_y^3 + 3 p_y v_y + \frac{6}{5} q_y + m_{yyy} \\ \rho v_x v_y^2 + p_y v_x + 2\sigma v_y + \frac{2}{5} q_y + m_{xyy} \\ Q_x v_y + Q_y v_x - E v_x v_y + M_{xxy} v_x + M_{xyy} v_y + \frac{1}{2}\left(\sigma v^2 + \bar{R}_{xy}\right) \\ 2 Q_y v_y - E v_y^2 + M_{xyy} v_x + M_{yyy} v_y + \frac{1}{2}\left(p_y v^2 + \bar{R}_{yy}\right) \end{pmatrix} \tag{37}$$

for the y-direction. Here, we also used $M_{ijk} = \frac{6}{5}\delta_{(ij} q_{k)} + m_{ijk}$, with the relevant components

$$M_{xxx} = \frac{6}{5} q_x + m_{xxx},\ M_{xxy} = \frac{2}{5} q_y + m_{xxy},\ M_{xyy} = \frac{2}{5} q_x + m_{xyy},\ M_{yyy} = \frac{6}{5} q_y + m_{yyy} \tag{38}$$

A detailed inspection shows the strong structural relation between F and G.

The fluxes require the values of m_{ijk} and $\bar{R}_{ij} = R_{ij} + \frac{1}{3} R \delta_{ij}$. Using tensorial identities the expressions in (11) give in explicit two-dimensional notation

$$\begin{pmatrix} m_{xxx} \\ m_{xxy} \\ m_{xyy} \\ m_{yyy} \end{pmatrix} = -2\frac{\theta}{\nu} \begin{pmatrix} \frac{3}{5}\partial_x \sigma_x - \frac{2}{5}\partial_y \sigma \\ \frac{1}{3}\partial_y \sigma_x + \frac{8}{15}\partial_x \sigma - \frac{2}{15}\partial_y \sigma_y \\ \frac{1}{3}\partial_x \sigma_y + \frac{8}{15}\partial_y \sigma - \frac{2}{15}\partial_x \sigma_x \\ \frac{3}{5}\partial_y \sigma_y - \frac{2}{5}\partial_x \sigma \end{pmatrix} \tag{39}$$

with normal stresses $\sigma_x = p_x - p$ and $\sigma_y = p_y - p$, and

$$\begin{pmatrix} R_{xx} \\ R_{xy} \\ R_{yy} \end{pmatrix} = -4\frac{\theta}{\nu} \begin{pmatrix} \frac{5}{3}\partial_x q_x + \frac{2}{3}\partial_y q_y \\ \frac{1}{2}\left(\partial_x q_y + \partial_y q_x\right) \\ \frac{5}{3}\partial_y q_y + \frac{2}{3}\partial_x q_x \end{pmatrix} \tag{40}$$

which can be directly utilized in the flux functions. In the case $m_{ijk} = 0$ and $R_{ij} = 0$ the flux functions reduce to the non-regularized fluxes, called $F^{(0)}(W)$ and $G^{(0)}(W)$. These correspond to Grad's 13-moment-case in two dimensions.

Finally, the relaxational source is given by

$$P(W) = \begin{pmatrix} \mathbf{0} \in \mathbb{R}^4 \\ -\nu\,\sigma_x \\ -\nu\,\sigma_y \\ -\nu\,\sigma \\ -2\nu\left(\sigma v_y + \sigma_x v_x + \frac{2}{3} q_x\right) \\ -2\nu\left(\sigma v_x + \sigma_y v_y + \frac{2}{3} q_y\right) \end{pmatrix} \tag{41}$$

which completes the system (32).

3 Modeling of Boundary Conditions

Compared to hydrodynamics with the laws of Navier-Stokes and Fourier, the R13 equations have an extended set of variables and corresponding equations. Thus, the usual set of boundary conditions are insufficient for the new theory. In fact, new boundary conditions need to be derived from kinetic gas theory.

The lack of boundary conditions was a major obstacle in the usage of moment equations, even though already Grad was using wall conditions derived from kinetic gas theory, see Goldberg (1954) and Grad (1958). Only in recent years this approach was rediscovered by Gu and Emerson (2007) and subsequently extended and refined by Torrilhon and Struchtrup (2008a) and Gu and Emerson (2009).

3.1 Maxwell's Accommodation Model

It is important to realize that the Boltzmann equation in kinetic gas theory comes with a model for walls which is generally accepted as valid boundary condition. To be consistent with the characteristic theory of Boltzmann's equation, it is requires that only the incoming half of the distribution function (with $\mathbf{n}\cdot\mathbf{c} > 0$, $\mathbf{n}$ wall normal pointing into the gas) have to be prescribed. The other half is given by the process in the interior of the gas. The incoming half can be prescribed in an almost arbitrary way, incorporating the complex microscopic phenomena at the wall.

The most common boundary condition for the distribution is Maxwell's accommodation model first presented in Maxwell (1879). It assumes that a fraction $\chi \in [0,1]$ of the particles that hit the wall are accommodated at the wall and injected into the gas according to a distribution function of the wall f_W. This distribution function is further assumed to be Maxwellian

$$f_W(\mathbf{c}) = \frac{\rho_W/m}{\sqrt{2\pi\theta_W}^3} \exp\left(-\frac{(\mathbf{c}-\mathbf{v}_W)^2}{2\theta_W}\right) \tag{42}$$

with θ_W and $\mathbf{v}_W$ given by the known temperature and velocity of the wall. We assume that the wall is only moving in tangential direction such that $\mathbf{v}_w$ has no normal component. The "wall density" ρ_W follows from particle conservation at the wall. The remaining fraction $(1-\chi)$ of the particles are specularily reflected. Since the particles that hit the wall are described by a distribution function f_{gas} the reflected part will satisfy a analogous distribution function $f^{(*)}_{\text{gas}}$ which follows from f_{gas} with accordingly transformed velocities.

From this model the velocity distribution function $\tilde{f}(\mathbf{c})$ in the infinitesimal neighborhood of the wall is given by

$$\tilde{f}(\mathbf{c}) = \begin{cases} \chi\, f_W(\mathbf{c}) + (1-\chi)\, f_{\text{gas}}^{(*)}(\mathbf{c}) & \mathbf{n}\cdot(\mathbf{c}-\mathbf{v}_W) > 0 \\ f_{\text{gas}}(\mathbf{c}) & \mathbf{n}\cdot(\mathbf{c}-\mathbf{v}_W) < 0 \end{cases} \tag{43}$$

where $\mathbf{n}$ is the wall normal pointing into the gas. This boundary conditions is used in the majority of simulations based on Boltzmann equation or DSMC, see Bird (1998). The accommodation coefficient χ describes the wall characteristics and has to be given or measured. The case of $\chi = 0$ (specular reflection) represents the generalization of an adiabatic wall (no heat flux, no shear stress) to the kinetic picture.

A realistic wall interaction is too complex to be described by a single parameter like χ, hence, the physically accuracy of the accommodation model needs to be judged carefully. However, as a simple model it gives sufficient results in many cases.

3.2 Wall Conditions for R13

As a system of balance laws the regularized 13-moment-equations require boundary conditions for the normal component of the fluxes. However, a detailed investigation shows that not all normal component can be prescribed, see Torrilhon and Struchtrup (2008a). Only those fluxes with odd normal components are possible, which are v_n, σ_{tn}, q_n, m_{nnn}, m_{ttn}, and R_{tn}, where t and n denote tangential and normal tensor components with respect to the wall.

From the Maxwell accommodation model we obtain boundary conditions for these moments. The first three are related to classical slip and jump boundary conditions and read

$$\begin{aligned} v_n &= 0 \\ \sigma_{tn} &= -\beta\left(P\,V_t + \tfrac{1}{2}m_{tnn} + \tfrac{1}{5}q_t\right) \\ q_n &= -\beta\left(2P\,\Delta\theta + \tfrac{5}{28}R_{nn} + \tfrac{1}{15}R + \tfrac{1}{2}\theta\,\sigma_{nn} - \tfrac{1}{2}P\,V_t^2\right) \end{aligned} \tag{44}$$

where $\Delta\theta = \theta - \theta_W$ is the temperature jump at the wall and $V_t = v_t - v_t^W$ is the tangential slip velocity. Additionally,

$$P := \rho\,\theta + \frac{\sigma_{nn}}{2} - \frac{R_{nn}}{28\theta} - \frac{R}{120\theta} \tag{45}$$

and the properties of the wall are given by its temperature θ_W and velocity v_t^W and the modified accommodation coefficient

$$\beta = \chi/(2-\chi)\sqrt{2/(\pi\theta)}. \tag{46}$$

When neglecting the contributions of the moments m_{ijk} and R_{ij}, these conditions can also be used for the system of Navier-Stokes and Fourier. R13 requires more boundary conditions which are given by

$$\begin{aligned} m_{nnn} &= \beta\left(\tfrac{2}{5}P\,\Delta\theta - \tfrac{1}{14}R_{nn} + \tfrac{1}{75}R - \tfrac{7}{5}\theta\,\sigma_{nn} - \tfrac{3}{5}P\,V_t^2\right) \\ m_{ttn} + \tfrac{m_{nnn}}{2} &= -\beta\left(\tfrac{1}{14}(R_{tt} + \tfrac{R_{nn}}{2}) + \theta(\sigma_{tt} + \tfrac{\sigma_{nn}}{2}) - P\,V_t^2\right) \\ R_{tn} &= \beta\left(P\,\theta\,V_t - \tfrac{1}{2}\theta\,m_{tnn} - \tfrac{11}{5}\theta\,q_t - P\,V_t^3 + 6P\,\Delta\theta V_t\right) \end{aligned} \tag{47}$$

again containing $\Delta\theta$, V_t as well as P and β. In extrapolation of the theory the accommodation coefficients that occur in every equation of (44)/(47) could be chosen differently as suggested in Grad (1958). Different accommodation coefficients of the single moment fluxes, e.g., shear or heat flux, could be used to model detailed wall properties. However, more investigations and comparisons are required for such an approach.

The first condition above is the slip condition for the velocity, while the second equation is the jump condition for the temperature. They come in a generalized form with the essential part given by $\sigma_{tn} \sim V_t$ and $q_n \sim \Delta\theta$. In a manner of speaking, the other conditions can be described as jump conditions for higher moments which again relate fluxes and respective variables. In perfect analogy to the usual slip and jump conditions, the essential part is given by $R_{tn} \sim q_t$ and $m_{nnn} \sim \sigma_{nn}$. The additional terms in (44)/(47) are off-diagonal terms coupling all even (in index n) moments in the boundary conditions.

4 Slow and Steady-State Processes

Many non-equilibrium gas situations occur in micro-mechanical systems where the dimensions are so small such that the Knudsen number becomes significant. At the same time, these processes are slow and often steady, such that linearized equations are mostly sufficient. This also allows to derive analytical solutions which provide additional insight into the equations.

4.1 Non-Equilibrium Phenomena

The distance of 10 mean free pathes correspond to $1\,\mu m$ in Argon at atmospheric conditions. Hence, on the micrometer scale the Knudsen number for flows of Argon can easily be large than $Kn \approx 0.1$. In micro-channels for gases this leads to non-equilibrium effects that can not be described by classical hydrodynamic theories, see for example the text book by Karniadakis and Beskok (2001).

Fig. 3 shows a channel orientated along the x-axis with a gas flowing from left to right. The width of the channel is used as observation scale to compute the Knudsen number which in this case is $Kn \approx 0.1$, such that on average only 10 particle collisions occur from one wall to the other. Both walls have the same temperature of dimensionless unity and the channel is imagined to be infinitely long such that all fields vary only across the channel, that is, the coordinate y.

The red dots indicate schematically what behavior for the fields must be expected. For velocity and temperature (top row) the result of classical NSF is shown as dashed line for comparison. Both velocity and temperature show strong jumps at the boundary. That is, the gas does not stick at the wall but slips with a certain velocity, and the temperature of the gas at the wall is significantly higher than the wall temperature. Additionally, the figure shows the fields of the heat flux q_x parallel to the wall, that is, along the channel, and the normal stress σ_{yy}. The heat is flowing against the flow in the middle of the channel and with it at the wall, while the normal stress shows a nonlinear behavior. Note, that from a classical understanding of gas dynamics both quantities should be zero in this setting. There are no temperature variations along the channel, hence, no heat should be flowing. Similarly, the divergence of the velocity field is zero, which according

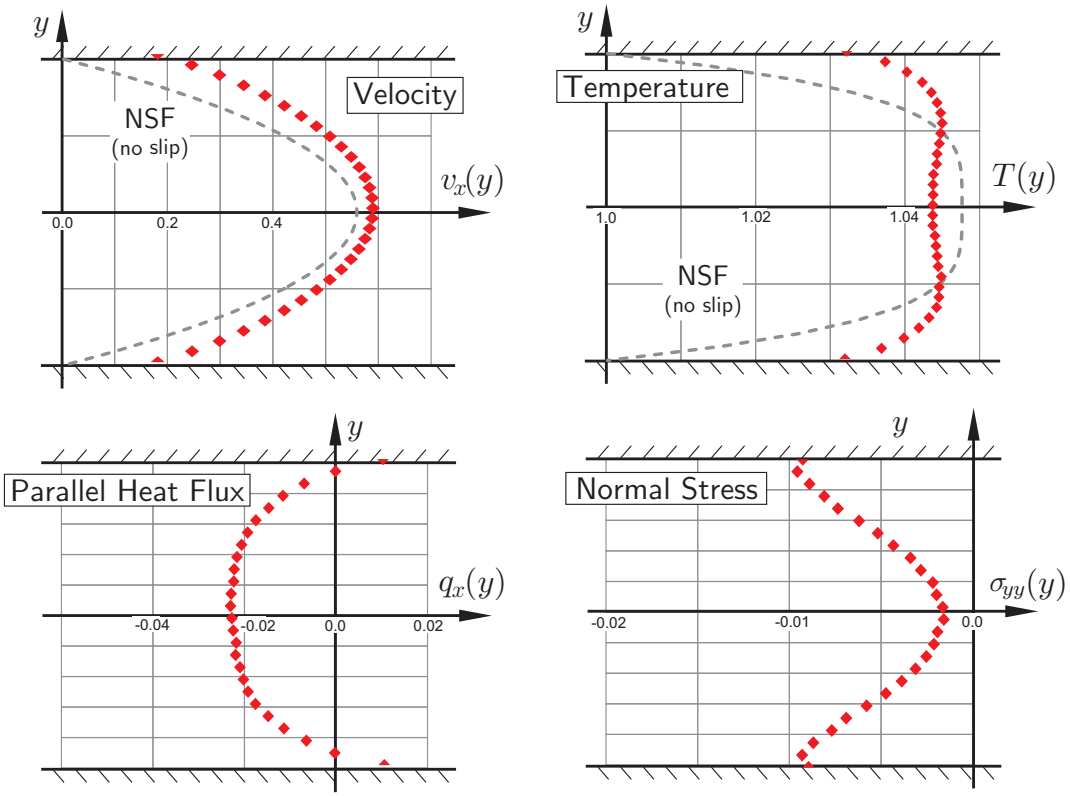

Figure 3: Exemplatory fields in channel flow for moderate Knudsen numbers ($Kn \approx 0.1$), showing non-gradient phenomena.

to the law of Navier-Stokes implies vanishing normal stresses. Still, the non-equilibrium triggers heat and stress effect without the presence of gradients. These phenomena are called non-gradient transport effects.

The temperature field in Fig. 3 also shows an interesting effect. Due to dissipation inside the flow, the gas in the channel is heated. This is a nonlinear effect and small due to the low speed of the flow. Fourier's law predicts a convex curve for the temperature (dashed line), while at large Knudsen numbers the temperature becomes non-convex with a dip in the middle of the channel. Note that, the normal heat flux (not shown) still shows only a single zero value in the middle of the channel and heat is flowing exclusively from the middle to the walls in contrast to the temperature gradient.

Another important feature of micro- or rarefied flows is the presence of Knudsen boundary layers. These boundary layers connect the interior bulk solution to the wall boundary typically on the scale of a few mean free pathes. Inside the layer the strong non-equilibrium induced by the contrast between the state of the wall and the gas situation relaxes exponentially to a balance between boundary condition and interior flow. For rarefied heat conduction between two walls this results in an s-shape temperature profile as shown on the right hand side of Fig. 4. The plot shows schematically the profile of temperature at $Kn \approx 0.1$ compared to the straight line of Fourier's law. On the left hand side the details of the Knudsen layers are given in a generic way. It is important to note that all fields of the flow exhibit such a layer in a more or less pronounced way. In a addition to the

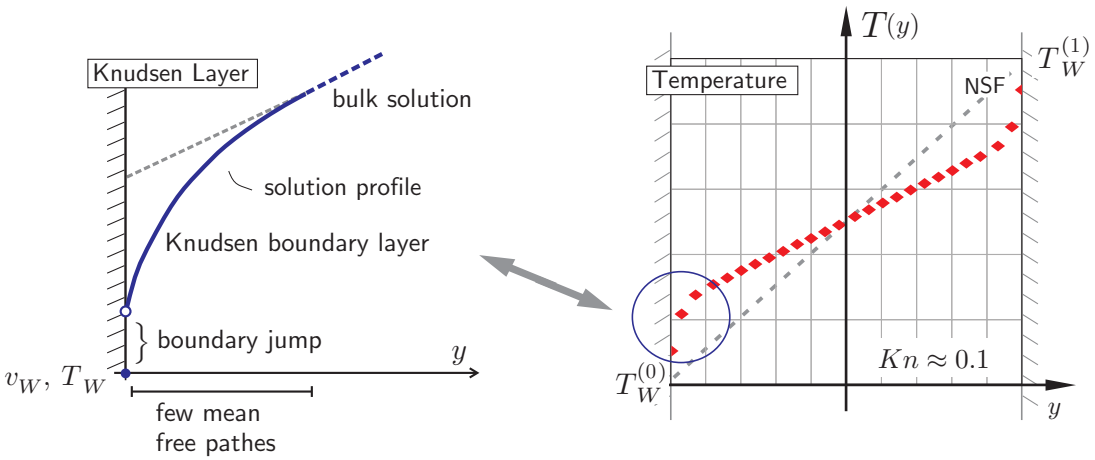

Figure 4: Schematic sketch of Knudsen layer close to the wall as a detail of the temperature field in an heat conduction experiment at moderate Knudsen numbers ($Kn \approx 0.1$).

Knudsen layer the fields of temperature and velocity jump at the wall to the respective wall value. Some boundary models neglect the Knudsen layer and incorporate its effect into an increased boundary jump. This is appropriate as long as the Knudsen layer can be separated from the bulk flow and does not influence the interior. The slip-flow regime ends before $Kn \approx 0.1$. In reality the fields of temperature and velocity always consist of a jump and Knudsen layer for *any* Knudsen number. However, the layer is squeezed into the wall and both its amplitude and the amplitude of the jump are proportional to Kn, hence, vanish in the hydrodynamic situation.

4.2 Linearized, Steady R13 System

To serve different preferences we will here present the equations in invariant formulation opposed to Cartesian index notation above.

4.2.1 Equations

The R13 equations describe the gas using the variables density ρ, velocity $\mathbf{v}$, temperature θ (in energy units $\theta = RT$), stress deviator $\boldsymbol{\sigma}$, and heat flux $\mathbf{q}$. The equation of state gives the pressure $p = \rho\,\theta$. In order to linearize the equations, we consider a ground state given by ρ_0, θ_0, and p_0, in which the gas is at rest and in equilibrium with vanishing stress deviator and heat flux. The linearized equations describe deviations from this ground state and from now on we use the variables $(\rho, \mathbf{v}, \theta, \boldsymbol{\sigma}, \mathbf{q})$ for these deviations. We will also allow an external force $\mathbf{F}$ acting on the gas.

The linearized conservation laws of mass, momentum and energy are then given by

$$\nabla \cdot \mathbf{v} = 0 \qquad \nabla p + \nabla \cdot \boldsymbol{\sigma} = \mathbf{F} \qquad \nabla \cdot \mathbf{q} = 0 \tag{48}$$

where $\mathbf{F}$ is the external force and the stress deviator and heat flux need to be specified.

For these the R13-system gives the constitutive relations

$$\frac{4}{5}(\nabla \mathbf{q})_{\text{sym}} + 2p_0(\nabla \mathbf{v})_{\text{sym}} = -\frac{p_0}{\mu_0}\boldsymbol{\sigma} + \frac{2\mu_0}{3\rho_0}\left(\Delta\boldsymbol{\sigma} + \frac{6}{5}\left((\nabla(\nabla\cdot\boldsymbol{\sigma}))_{\text{sym}} - \frac{1}{3}\nabla\cdot(\nabla\cdot\boldsymbol{\sigma})\mathbf{I}\right)\right) \tag{49}$$

$$\theta_0\nabla\cdot\boldsymbol{\sigma} + \frac{5}{2}p_0\nabla\theta = -\frac{2p_0}{3\mu_0}\mathbf{q} + \frac{6\mu_0}{5\rho_0}\Delta\mathbf{q} \tag{50}$$

where the parameter μ_0 is the viscosity of the gas at ground state. As described above, these equations involve differential operators for stress and heat flux. Hence, the conservation laws (48) must be solved together with (49)/(50) as a coupled system of partial differential equations. In (49) we use the notation $(A)_{\text{sym}} = \frac{1}{2}(A + A^T)$ for matrices A. Note that $\nabla(\nabla\cdot\boldsymbol{\sigma})$ is the gradient of the divergence of the stress deviator and as such a matrix. We view the conservation laws as equations for pressure, velocity and temperature. The density can be computed from the solution by means of the equation of state. In contrast to the presentation of the R13 equations above, here we inserted the relation for the higher order fluxes directly into the equations for stress and heat flux.

The viscosity gives rise to the mean free path λ_0 in the gas at ground state from which we define the Knudsen number by

$$Kn = \lambda_0/L \quad \text{with } \lambda_0 = \frac{\mu_0\sqrt{\theta_0}}{p_0} \tag{51}$$

using a macroscopic length scale L. As above, an asymptotic expansion reduces the constitutive laws (49)/(50) to

$$\boldsymbol{\sigma}^{(\text{NSF})} = -2\mu_0(\nabla\mathbf{v})_{\text{sym}}, \qquad \mathbf{q}^{(\text{NSF})} = -\frac{15}{4}\mu_0\nabla\theta \tag{52}$$

with which the conservation laws turn into

$$\nabla\cdot\mathbf{v} = 0, \qquad \nabla p = \mu_0\Delta\mathbf{v}, \qquad \Delta\theta = 0, \tag{53}$$

that is, the Stokes equations and a separate Laplace equation for the temperature. The steady, linear R13 equations can be viewed as an extension of the Stokes equations which couple the flow and temperature problem.

4.2.2 Wall Boundary Conditions

At an impermeable wall at rest the linear R13 equations have to satisfy the boundary conditions as given above. Here we give the linearized version. First, we have generalized velocity slip and temperature jump conditions

$$\sigma_{nt} = -\frac{\tilde{\chi}}{\sqrt{\theta_0}}\left(p_0\, v_t + \frac{1}{5}q_t + \frac{1}{2}m_{nnt}\right) \tag{54}$$

$$q_n = -\frac{\tilde{\chi}}{\sqrt{\theta_0}}\left(2p_0(\theta - \theta_W) + \frac{1}{2}\theta_0\,\sigma_{nn} + \frac{5}{28}R_{nn}\right) \tag{55}$$

which in the case of R13 are written using the variables shear stress and normal heat flux instead of velocity and temperature gradient. They also involve components of higher

order moments. Again, the index t denotes the component of a tensor in the direction of the tangential flow at the wall, while n is the component normal to the wall. The coefficient $\tilde{\chi}$ is given by $\tilde{\chi} = \sqrt{\frac{2}{\pi}}\frac{\chi}{2-\chi}$, where χ is the accommodation coefficient of the wall model as discussed above. In the following, $\chi = 1$, that is, $\tilde{\chi} = \sqrt{2/\pi} \approx 0.798$, for full accommodation will be used.

In addition to the classical slip and jump condition the R13 system requires generalized slip and jump conditions for the heat flux and stress tensor

$$R_{nt} = -\frac{\tilde{\chi}}{\sqrt{\theta_0}}\left(-\theta_0 p_0 \theta_0\, v_t + \frac{11}{5}\theta_0\, q_t + \frac{1}{2}\theta_0\, m_{nnt}\right) \tag{56}$$

$$m_{nnn} = -\frac{\tilde{\chi}}{\sqrt{\theta_0}}\left(-\frac{2}{5}p_0(\theta - \theta_W) + \frac{7}{5}\theta_0\, \sigma_{nn} + \frac{1}{14}R_{nn}\right) \tag{57}$$

$$m_{ntt} - m_{nss} = -\frac{\tilde{\chi}}{\sqrt{\theta_0}}\left(\frac{R_{tt} - R_{ss}}{14} + \theta_0(\sigma_{tt} - \sigma_{ss})\right) \tag{58}$$

which involve the higher order moments $\mathbf{R}$ and $\mathbf{m}$. The components of the direction orthogonal to these two directions will be denoted by index s. These are given as gradients of heat flux and stress by

$$\mathbf{R} = -\frac{24}{5}\frac{\mu_0}{\rho_0}(\nabla \mathbf{q})_{\text{sym}}, \tag{59}$$

$$\mathbf{m} = -2\frac{\mu_0}{\rho_0}(\nabla \boldsymbol{\sigma})_{\text{sym+tracefree}}. \tag{60}$$

Note, that $\mathbf{R}$ is a symmetric and tracefree 2-tensor, according to $(48)_3$, while $\mathbf{m}$ is a symmetric and tracefree 3-tensor. A general definition and discussion of this tensor can be found in Struchtrup (2005b). Some components can also be found in Torrilhon (2010b). Finally, the velocity at an impermeable wall has to satisfy

$$v_n = 0. \tag{61}$$

In total, this gives five linear conditions on a wall for the R13 system.

4.3 Channel Flow

The easiest internal flow to consider is a channel flow between to infinite plates at a distance of L, see Fig. 5. The x-axis will be in the middle of the channel such that the walls reside at $y = \pm L/2$. The Knudsen number is based on the channel width L. We will assume that the plates are at rest and equal temperature. A constant driving force F is given in the direction of the channel, interpreted as a pressure difference or rather a body force like gravity if the channel is imagined as standing upright. We are interested in the steady profiles of the flow fields. Due to the simple geometric set-up the fields will only depend on the variable y across the channel and show no variation in x-direction along the channel. This considerably simplifies the R13 system.

The following variables and equations are utilized in non-dimensional form where all variables are scaled with ρ_0 and powers of $\sqrt{\theta_0}$, and space is scaled by the channel width L. The equations contain as parameters only the Knudsen number and the dimensionless force which is scaled by $F_0 = \rho_0\theta_0/L$.

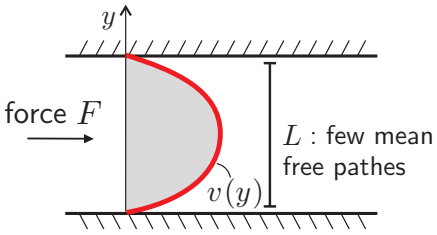

Figure 5: Channel Setup: Infinite extension in x-direction, all fields depend only on coordinate y.

4.3.1 Flow Field

The flow field is governed by two variables: the velocity profile along the channel v_x, and the shear stress σ_{xy}. The relevant component of the momentum balance reads

$$\partial_y \sigma_{xy} = F \tag{62}$$

and for σ_{xy} we have the equation

$$\frac{2}{5}\,\partial_y q_x + \partial_y v_x = -\frac{1}{Kn}\sigma_{xy} \tag{63}$$

containing the law of Navier-Stokes. However, in the R13 equations a gradient of the tangential heat flux q_x influences the shear stress in the same way as the derivative of the velocity v_x. Accordingly, this heat flux influences the profile of velocity which can be computed as

$$v_x\,(y) = C_1 + \frac{F}{2Kn}\left(\frac{1}{4} - y^2\right) - \frac{2}{5}q_x\,(y) \tag{64}$$

with a integration constant C_1 to be fixed by boundary conditions. In this result the classical parabolic profile is perturbed by the tangential heat flux. For constant dimensionless force F the amplitude of the parabolic profile increases with smaller Knudsen number. This corresponds to a less viscous flow with large velocity due to reduced friction. On the other hand, higher Knudsen numbers decrease the classical velocity profile due to viscous friction.

There is no reason to assume a vanishing tangential heat flux, instead the R13 equation for q_x reads

$$\partial_y \sigma_{xy} = -\frac{2}{3}\frac{1}{Kn}q_x + \frac{6}{5}Kn\,\partial_{yy} q_x \tag{65}$$

where the derivative of the shear stress can be substituted with the force F. After multiplication with Kn this equation shows that the magnitude of q_x reduces with Kn and hence, the tangential heat flux is a non-equilibrium effect. The equation for q_x allows for nontrivial solutions without the presence of a temperature gradient. The result is a nongradient transport effect. The second order differential operator gives exponential solutions of the form $C_\pm \exp\left(\pm y/Kn\right)$ with integration constants $C_\pm$. These parts of the solution decay towards the interior and are identified with the Knudsen layer at the boundary. The boundary conditions fix the amplitude of the Knudsen layer. The bulk

solution of the tangential heat flux is a constant given by the left hand side of the equation and the total solution is

$$q_x(y) = -\frac{3}{2} Kn\, F + C_2 \cosh\left(\frac{\sqrt{5/9}}{Kn} y\right) \tag{66}$$

where due to symmetry the exponential functions of the Knudsen layer are incorporated into the cosh. This solution gives a negative offset for q_x in the middle of the channel and layer behavior at the boundaries. Note, that this is precisely the behavior of the parallel heat flux in Fig. 3. The bulk solution is directly related to the force. The integration constant will be proportional to Kn such that q_x vanishes in near equilibrium flows. However, for larger Knudsen numbers the exponential layers from both boundaries grow into each other and q_x shows a non-linear behavior everywhere in the channel. The result suggests that the heat flux with the flow is automatically triggered from any shear flow at higher Knudsen numbers even in absence of temperature differences. However, heat is flowing - in the current equations from one end of the channel to the next. Due to the infinite extension no temperature difference can be produced, but we will see below that in finite geometry interesting temperature pattern can occur.

The complete solution of q_x is superimposed to the velocity profile in (64). It inherits its Knudsen number to the velocity profile, however, due to the parabolic behavior these layers are hardly visible, for example in Fig. 3.

As boundary conditions we prescribe the flux of momentum σ_{xy} and the flux of heat flux R_{xy} as given in (54) and (56). These are two conditions for the two integration constants $C_{1,2}$. The first one represents the slip condition for v_x. We will not give the full expressions for these constants but only remark the the result is fully explicit only depending on the accommodation coefficient of the wall.

4.3.2 Temperature Profile

Any flow generates heat through dissipation leading to a temperature rise in general. In slow channel flows the heating effect is small and when linearizing the equations the dissipation rate $r(y) = -\sigma_{xy}\partial_y v_x$, present in the energy balance drops out as quadratic expression. As a result the linearized R13 equations predict a constant temperature.

In order to investigate the temperature increase we will insert the dissipation rate computed from the classical part of the flow field (64)

$$r(y) = -\sigma_{xy}\partial_y v_x = \frac{F^2}{Kn} y^2 \tag{67}$$

as heat source in the energy equation, but the rest of the equations remain linear for simplicity. That is, we have the energy balance

$$\partial_y q_y = r(y) \tag{68}$$

and the R13 equation for the normal heat flux

$$\partial_y \sigma_{yy} + \frac{5}{2}\partial_y \theta = -\frac{2}{3}\frac{1}{Kn} q_y \tag{69}$$

which contains Fourier's law. Analogously to the flow equations above, the heat flux couples to an atypical quantity which is the normal stress σ_{yy}. Any result for the normal stress is superimposed on the temperature solution according to

$$\theta(y) = C_3 - \frac{1}{45}\frac{F^2}{Kn^2}y^4 - \frac{2}{5}\sigma_{yy}(y). \tag{70}$$

For $\sigma_{yy} = 0$ this is the classical temperature profile in Poiseuille flow due to dissipation. Due to symmetry there is only one integration constant C_3 which follows from boundary condition for temperature. The temperature profile is a quartic polynomial with maximum in the middle of the channel. It is quadratic in the force which identifies the temperature increase as nonlinear effect.

There is no reason to assume $\sigma_{yy} = 0$, instead the R13 equation for stress gives us

$$\frac{4}{5}\partial_y q_y = -\frac{1}{Kn}\sigma_{yy} + \frac{6}{5}Kn\,\partial_{yy}\sigma_{yy} \tag{71}$$

which has the same structure as the equation for the tangential heat flux, namely a second order operator with forcing that stems from the conservation law. The solution for σ_{yy} consists of a bulk solution directly related to the dissipation rate and exponential layer

$$\sigma_{yy}(y) = -\frac{48}{25}F^2Kn^2 - \frac{4}{5}F^2y^2 + C_4\cosh\left(\frac{\sqrt{5/6}}{Kn}y\right). \tag{72}$$

Again, this layer is identified as Knudsen layer with an amplitude controlled by an integration constant. The final shape of the normal stress is an up-side-down parabola shifted downwards. The layers have positive amplitudes and produce upward kinks towards the boundaries. This corresponds to the shape of σ_{yy} given in Fig. 3. Similar to the tangential heat flux the normal stress is triggered by the heat conduction at larger Knudsen numbers without parallel gradients of velocity like $\partial_y v_y$.

The normal stress enters the temperature profile (70) with opposite sign. This means that the classical quartic shape is competing with an upward parabola. The quartic is reduced with larger Knudsen numbers, thus, the temperature becomes dented in the middle and a non-convex shape arises. This explains the plot in Fig. 3. Note that the normal heat flux q_y remains a cubic polynomial with single zero in the middle for all Knudsen numbers. Hence, within the dent of the temperature profile heat flows from cold to warm in contradiction to Fourier's law - which, of course, is not valid at these Knudsen numbers.

4.3.3 Full Simulation

The R13 equations have been solved for Poiseuille flow in the full non-linear case numerically in Torrilhon and Struchtrup (2008a) and analytical results for semi-linearized equations are investigated in Taheri et al. (2009). The analytical computations follow the line of thinking of the presentation above but include more non-linear terms than only the dissipation in the energy balance.

Fig. 6 presents numerical solutions of the nonlinear R13 equations for various Knudsen numbers with a dimensionless acceleration force fixed at $F = 0.23$ and viscosity exponent

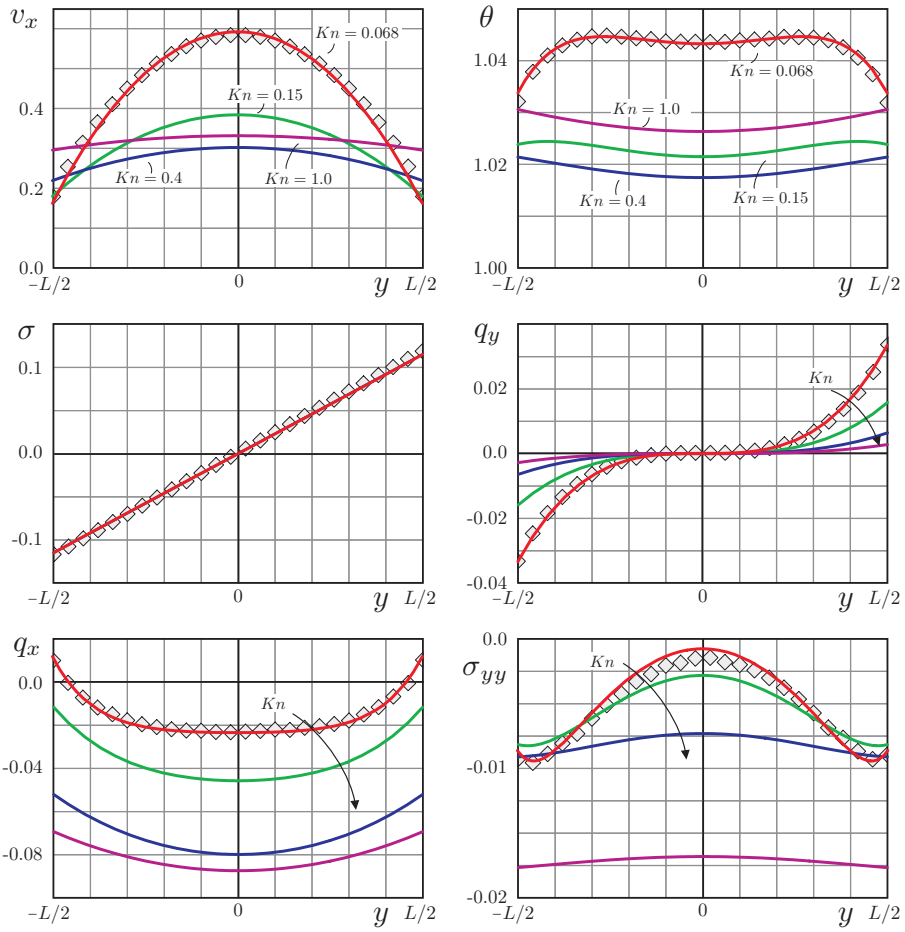

Figure 6: Results of nonlinear R13 for slow Poiseuille flow with various Knudsen numbers.

$\omega = 0.5$. These values are chosen such that a Knudsen number $Kn = 0.068$ reproduces the case of Poiseuille flow calculated in Zheng et al. (2002) (see also Xu and Li (2004)) by DSMC. We also calculate the cases $Kn = 0.15$, 0.4, 1.0. The figure displays the results for all Knudsen numbers together with the DSMC solution for $Kn = 0.068$. The figure shows the fluid variables velocity and temperature, their fluxes stress σ and heat flux q_y, as well as the rarefaction variables tangential heat flux q_x and normal stress σ_{yy}. All variables are reproduced as smooth curves without any tendencies to oscillate even when the grid is refined. Higher Knudsen numbers show stronger non-equilibrium as indicated by larger magnitudes of q_x and σ_{yy}. Interestingly, the temperature profile is not only dented but starts to invert for higher Knudsen numbers. This has still to be confirmed by DSMC calculations.

The rarefied flow through a channel is known to exhibit a paradoxical behavior known as Knudsen paradox, see Knudsen (1909), which is also observed in kinetic simulations, for instance in Sharipov and Seleznev (1998). When reducing the Knudsen number in the experiment the normalized mass flow rate

$$J = \int_{-1/2}^{1/2} v(y)\, dy \tag{73}$$

through the channel reaches a minimum and afterwards starts to increase for larger Knudsen numbers. Intuitively one would expect a decreasing mass flow for a smaller channel, but at a certain scale the friction inside the gas becomes so small that the growing slip velocity at the wall dominates the mass flow. This can also be observed in the results of the R13-system in Fig. 6. The velocity profile becomes flatter, but the slip increases and the velocity curve for $Kn = 1.0$ lies above the curve of $Kn = 0.4$. Qualitatively, this shows that the R13 equations are able to describe the Knudsen paradox, however, the error in the prediction of the mass flow rate becomes significant beyond $Kn = 1.0$, see Torrilhon and Struchtrup (2008a).

Note that the Knudsen paradox is mainly a phenomenon introduced by the boundary slip. Hence, it is possible to tune the boundary conditions of the system of Navier-Stokes and Fourier such that the velocity shows this paradoxical behavior, see e.g., Hadjiconstantinou (2003) and Struchtrup and Torrilhon (2008).

4.4 Flow Around a Sphere

The flow around a sphere is a classical example for exterior flow. We consider the setup depicted in Fig. 7 in spherical coordinates. The sphere has radius R. The flow is coming from the left and the symmetry axes is aligned with the flow such that the flow pattern is identical in any section along φ. The temperature of the sphere and of the flow at infinity is θ_0.

We will assume slow flow which means low Mach number $M_0 = v_0/c_0$ with isothermal speed of sound $c_0 = \sqrt{\theta_0}$. This assumption allows us to us linearized the field equations. In classical hydrodynamics an analytical result for the flow field has been given by Stokes (1842) and became standard material in text books, e.g., Batchelor (2000) or Lamb (1993). In Torrilhon (2010b) it is shown that an analytical result is also possible for the linearized R13 equation.

4.4.1 Analytic Solution

According to Fig. 7 we will seek a solution for the linearized R13 equations in spherical coordinates, such that the fields only depend on r and ϑ but not on φ. Furthermore we will use separation of variables in an ansatz with explicit dependence in the angle ϑ. The ansatz is inspired from the classical Stokes solution. This gives for the spherical coordinates of velocity $\mathbf{v} = (v_r, v_\vartheta, v_\varphi)$ the form

$$\mathbf{v}(r,\vartheta) = v_0 \begin{pmatrix} \left(1 + a(\frac{r}{R})\right)\cos\vartheta \\ -\left(1 + b(\frac{r}{R})\right)\sin\vartheta \\ 0 \end{pmatrix} \tag{74}$$

and for temperature and pressure

$$\theta(r,\vartheta) = \theta_0\, c(\frac{r}{R})\cos\vartheta, \quad p(r,\vartheta) = p_0\, d(\frac{r}{R})\cos\vartheta, \tag{75}$$

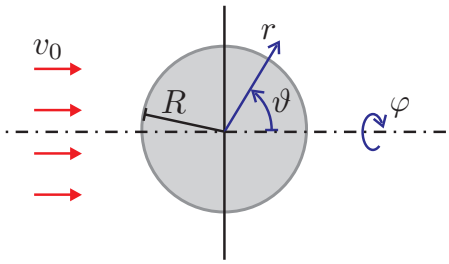

Figure 7: Geometric setup for the flow around a sphere with inflow from the left and identical flow pattern for each section along φ.

with unknown functions $a(x)$, $b(x)$, $c(x)$, and $d(x)$, where $x = r/R$. For the spherical coordinates of heat flux and stress we use

$$\mathbf{q}(r,\vartheta) = p_0\sqrt{\theta_0}\begin{pmatrix} \alpha(\frac{r}{R})\cos\vartheta \\ -\beta(\frac{r}{R})\sin\vartheta \\ 0 \end{pmatrix}, \quad \boldsymbol{\sigma}(r,\vartheta) = p_0\begin{pmatrix} \gamma(\frac{r}{R})\cos\vartheta & \kappa(\frac{r}{R})\sin\vartheta & 0 \\ \kappa(\frac{r}{R})\sin\vartheta & \sigma_{\vartheta\vartheta} & 0 \\ 0 & 0 & \sigma_{\varphi\varphi} \end{pmatrix} \tag{76}$$

with unknown functions $\alpha(x)$, $\beta(x)$, $\gamma(x)$, $\kappa(x)$ and $\sigma_{\varphi\varphi} = \sigma_{\vartheta\vartheta} = -\sigma_{rr}/2$ to ensure a tracefree stress deviator. If this ansatz is inserted into the R13 system we can extract 8 ordinary differential equations for the 8 unknown functions $\psi = (a, b, c, d, \alpha, \beta, \gamma, \kappa)$.

The solution $\psi(x)$ is of the form

$$\psi(x) = \psi_0(x) + \psi_1(x)\exp\left(-\lambda_1(x-1)\right) + \psi_2(x)\exp\left(-\lambda_2(x-1)\right) \tag{77}$$

where $\psi_{0,1,2}(x)$ are polynomials in $1/x$. The first part $\psi_0(x)$ represents the bulk solution while $\psi_{1,2}(x)\exp\left(-\lambda_{1,2}(x-1)\right)$ describe the exponential boundary layers which vanish away from the wall for $x \gg 1$. Only two layers are present in the R13 theory and in the current setting they can be identified to originate from β, that is, the angular or tangential heat flux, and γ, which is the radial normal stress. This reproduces the theme already known from the channel flow computations.

It turns out that the Knudsen layers introduced by β and γ, each influence only a separate part of the solution. The Knudsen layer of the angular heat flux β is present in the radial heat flux α and both velocity components a and b. Their solution is given by

$$a(x) = C_1\frac{1}{2x} + C_2\frac{1}{3x^3} - K_1\left(\frac{6Kn^3}{5x^3} + \frac{2}{\sqrt{5}}\frac{Kn^2}{x^2}\right)e^{-\sqrt{\frac{5}{9}}\frac{x-1}{Kn}} \tag{78}$$

$$b(x) = C_1\frac{1}{4x} - C_2\frac{1}{6x^3} + K_1\left(\frac{3Kn^3}{5x^3} + \frac{Kn^2}{\sqrt{5}x^2} + \frac{Kn}{6x}\right)e^{-\sqrt{\frac{5}{9}}\frac{x-1}{Kn}} \tag{79}$$

$$\frac{\alpha(x)}{M_0} = C_3\frac{Kn}{6x^3} - C_1\frac{3Kn^2}{2x^3} + K_1\left(\frac{3Kn^3}{x^3} + \sqrt{5}\frac{Kn^2}{x^2}\right)e^{-\sqrt{\frac{5}{9}}\frac{x-1}{Kn}} \tag{80}$$

$$\frac{\beta(x)}{M_0} = -C_3\frac{Kn}{12x^3} + C_1\frac{3Kn^2}{4x^3} - K_1\left(\frac{3Kn^3}{2x^3} + \sqrt{5}\frac{Kn^2}{2x^2} + \frac{5Kn}{6x}\right)e^{-\sqrt{\frac{5}{9}}\frac{x-1}{Kn}} \tag{81}$$

where wall boundary conditions at the sphere surface have not yet been employed. The Knudsen layer of the radial normal stress γ occurs in the shear stress κ, the temperature

c and the pressure d. The solutions read

$$\frac{c(x)}{M_0} = C_3\frac{1}{45x^2} + K_2\left(\sqrt{\frac{6}{5}}\frac{2Kn^2}{x^2} + \frac{2Kn}{x}\right)e^{-\sqrt{\frac{5}{6}}\frac{x-1}{Kn}} \tag{82}$$

$$\frac{d(x)}{M_0} = C_1\frac{Kn}{2x^2} + K_2\left(\frac{\sqrt{30}Kn^2}{x^2} + \frac{5Kn}{x}\right)e^{-\sqrt{\frac{5}{6}}\frac{x-1}{Kn}} \tag{83}$$

$$\begin{aligned}\frac{\gamma(x)}{M_0} &= C_1\frac{Kn}{x^2} + C_2\frac{2Kn}{x^4} + (C_3 - 25C_1Kn)\frac{2Kn^2}{5x^4} \\ &\quad - K_2\left(\sqrt{\frac{6}{5}}\frac{54Kn^4}{x^4} + \frac{54Kn^3}{x^3} + \frac{4\sqrt{30}Kn^2}{x^2} + \frac{5Kn}{x}\right)e^{-\sqrt{\frac{5}{6}}\frac{x-1}{Kn}}\end{aligned} \tag{84}$$

$$\begin{aligned}\frac{\kappa(x)}{M_0} &= C_2\frac{Kn}{x^4} + (C_3 - 25C_1Kn)\frac{Kn^2}{5x^4} \\ &\quad - K_2\left(\sqrt{\frac{6}{5}}\frac{27Kn^4}{x^4} + \frac{27Kn^3}{x^3} + \sqrt{\frac{15}{2}}\frac{3Kn^2}{x^2}\right)e^{-\sqrt{\frac{5}{6}}\frac{x-1}{Kn}}\end{aligned} \tag{85}$$

again without wall boundary conditions.

In this solution the classical Stokes solution is color-coded in blue and green. Blue gives the flow solution and green the heat conduction process. This solution is governed by three integration constants $C_{1,2,3}$ which are essentially computed from the classical slip and jump condition and the impermeability condition of the wall. Note that $C_{1,2}$ are related to the velocity field and stress, while C_3 is present in temperature and heat flux. The latter constant is zero in the Stokes solution resulting in a uniform temperature.

R13 adds two contributions to the flow around a sphere. The most pronounced contribution is the existence of Knudsen layers. Inside the layers the coupling of the fields is counter-intuitive. As indicated by the integration constants $K_{1,2}$ the velocity couples to heat flux, while temperature couples to stress tensor. The amplitude of the heat flux layer is governed by the boundary condition for the flux of heat flux $R_{r\vartheta}$, the stress layer is controlled by the boundary condition for m_{rrr}. Note that there is some coupling between the layers via the boundary conditions.

Next to the Knudsen layers R13 also adds changes to the bulk solution. These are color-coded in red in the above solutions and also appear in a counter-intuitive way. Inspecting the constants $C_{1,2,3}$ the heat flux bulk solution is influence from the velocity, and the stress is influenced by the temperature solution. Hence, both through the Knudsen layer and the bulk solution the heat flux behaves independent from the temperature gradient. Due to this decoupling heat may flow from cold to warm as we will see below.

The constants $C_{1,2,3}$ and $K_{1,2}$ depend only on the Knudsen number and the accommodation coefficient χ. Note that, especially $C_{1,2,3}$ will not have the same values as in the Stokes solution due to the coupling in the boundary conditions. The classical values are recovered for $Kn \to 0$ which gives $C_1 = -3$, $C_2 = 1.5$, $C_3 = 0$. The Knudsen layer solution $\psi_{1,2}$ is proportional to Kn and vanishes for $Kn \to 0$.

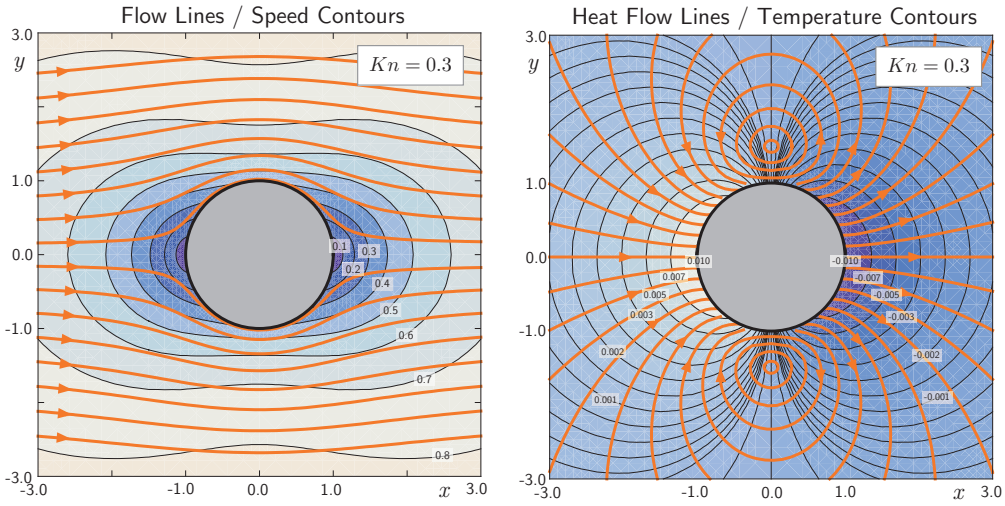

Figure 8: Stream and heat lines for the flow past a sphere at $Kn = 0.3$ computed with R13.

4.4.2 Stream and Heat Lines

The left hand side of Fig. 8 shows the stream lines and the speed contours (amplitude of velocity) of the R13 result for the case $Kn = 0.3$ with accommodation coefficient $\chi = 1$. The flow line pattern is very similar to the classical Stokes result, however, in the R13 case slip flow on the wall is visible and the flow has a wider influence above and below the sphere.

It is an interesting aspect of the solution of the R13 system that it predicts temperature variations and heat flow in the flow around a sphere. The heat flow lines together with temperature contours are shown at the right hand side of Fig. 8 for $Kn = 0.3$. Note, that the flow is considered slow and the result is based on linearized equations. Hence, quadratic energy dissipation typically responsible for temperature increase through shear, is not present. The temperature variations predicted by R13 are the result of the coupling of stress and heat flux equations in (49)/(50) which take effect for larger values of the Knudsen number. This effect has to be related to the tangential heat flux in channel flows triggered by shear stress. The flow around the sphere triggers a parallel heat flux in a similar way. While in the channel the heat is swept from minus infinity to plus infinity, for the sphere real temperature variations occur.

As can be seen in Fig. 8 the temperature increases in front and decreases in the back of the sphere. Such a temperature polarization is known for rarefied or micro-flows around obstacles and the result of the R13 equations is in agreement with the findings of Takata et al. (1993) on the basis of the linearized Boltzmann equation. All quantities in the R13 result, except velocity, are proportional to the Mach number of the inflow M_0. The contour level values on the right hand side of the figure must be multiplied with M_0 to obtain the relevant temperature deviations for a specific case. The maximal temperature increase at the front of the sphere is $0.01\, M_0\, \theta_0$ for $Kn = 0.3$.

On top and below the heat flow forms recirculation areas which indicate the Knudsen layer. Outside this layer at approximately $r = 1.8$ the heat flux essentially flows from the back in big loops to the front of the sphere, in contrast to the intuition based on

the temperature gradient. This is possible since the bulk solution for heat flux as given above contains terms not linked to the temperature gradient, a so-called non-gradient transport effect. While the sign of the temperature polarization corresponds to the full Boltzmann solution in Takata et al. (1993), no heat flux result for Boltzmann is given in the literature. Note, that the asymptotic expansion of Aoki and Sone (1987) for small Knudsen numbers predicts a higher temperature in the front, but this expansion is not valid in the case $Kn = 0.3$. In the R13 result the temperature becomes positive for very small Knudsen numbers $Kn < 0.004$. Only then the hydrodynamics limit is reached in which the heat flows against the temperature gradient.

5 Nonlinear Problems

The R13 equations have been derived from Boltzmann equation in with full non-linear expressions. Similarly, the boundary conditions follow nonlinearly without restriction. The nonlinear equations have been investigated and tested in several processes, but the state of development lacks behind the linearized R13 system. Many aspects of the nonlinear R13 equations are an acute field of research at present times.

We will present some results for nonlinear problems.

5.1 Shock Profiles

In a shock wave a gas experiences a fast transition between two equilibrium states across a domain of only few mean free paths. Due to the absence of boundary effects and because of its essential one-dimensionality, the normal shock wave is one of the simplest flows with large deviations from thermodynamical equilibrium. Hence, the shock structure became a popular and challenging benchmark problem for testing theoretical descriptions of non-equilibrium and rarefied flows.

Shock waves are modeled as fully one-dimensional. Hence, velocity, stress deviator and heat flux have only a single non-trivial component in the direction normal to the shock wave. Note that, the stress tensor is diagonal, but the diagonal entries are related by $\sigma_{33} = \sigma_{22} = -\sigma_{11}/2$. The shock profile smoothly connects the equilibrium states of density ρ_0, velocity v_0, and temperature T_0 before the shock at $x \to -\infty$ with the equilibrium ρ_1, v_1, T_1 behind the shock at $x \to \infty$. The Rankine-Hugoniot conditions implied by the conservation laws relate the values before and after the shock. The flow can be assumed steady in which the inflow v_0 represents the shock speed. The density and temperature are increasing through the shock while the velocity (in the steady picture from left to right) is reduced by the shock.

Fundamental measurements of complete shock structures have been accurately conducted and furnish data for theoretical results to compare with. By choosing a statistical particle approach the experimental data have been satisfactory reproduced in DSMC calculations, see Bird (1998). However, so far no rational continuum description of rarefied flow succeeded to predict the experimental evidence accurately over a significant range of the shock wave Mach number. The Mach number is defined as $M_0 = v_0/a_0$ from the shock velocity v_0 and the sound velocity a_0 in front of the shock. Classical theories like the equations of Navier-Stokes and Fourier succeed to predict at least the shock thickness

qualitatively, see Gilberg and Paolucci (1953), but the quantitative agreement is restricted to Mach numbers up to $M_0 \approx 1.3$. Even worse, the NSF theory can not even reproduce the shock asymmetry qualitatively, as shown in Alsmeyer (1976), Pham-Van-Diep et al. (1991) and Au (2001). These results reflect the fact that the NSF equations are restricted to describe near equilibrium flows.

Within the framework of kinetic theory several extensions to the theory of NSF have been derived by means of the Chapman-Enskog expansion, yielding the Burnett and Super-Burnett equations. Unfortunately, these higher order theories suffer from instabilities which result in oscillatory solutions for shock structures, see e.g. Uribe et al. (1998) and Zhong et al. (1993). The moment method proposed by Grad (1949) also tries to approach the shock wave problem. Grad's 13-moment-case was derived as improvement of the NSF theory in the description of rarefied flows. Unfortunately, the equations describes the shock thickness only up to $M_0 \approx 1.1$ accurately and beyond Mach number $M_0 = 1.65$ they fail to describe continuous shock structures, since they suffer from a subshock in front of the shock, see Grad (1952). This subshock grows with higher Mach numbers and at $M_0 \approx 3.5$ a second subshock appears in the middle of the shock. Both subshocks are artefacts from the hyperbolic nature of the 13-moment equations Torrilhon (2000). It turned out that any hyperbolic moment theory will yield continuous shock structures only up the Mach number corresponding to the highest characteristic velocity, see Ruggeri (1993) and Weiss (1995). Nevertheless, the moment method is capable of describing shock structures accurately provided sufficiently many moments are considered, which is shown in Weiss (1995) and Au (2001).

One of the reasons to derive new 13-moment-equations in Struchtrup and Torrilhon (2003) was to obtain field equations which lead to smooth and stable shock structures for any Mach number. Since the equations are based on Grad's 13-moment-case, it must be emphasized that quantitative accuracy of the R13-solutions is *still restricted* to small Mach numbers. However, the range of validity is extended by including higher order expansion terms into the R13 equations.

Fig. 9 compares the shock profiles for velocity obtained from Grad's 13-moment-case and R13 at $M_0 = 3.0$ arbitrarily shifted along the x-axis. The Grad profile shows a strong subshock in front of the shock and a kink towards the indicating the onset of a second subshock at higher Mach numbers. Adding higher order gradient expressions obtained from Boltzmann's equation to Grad's system leads to the R13 equations and a smooth shock profile. The diffusion added should not be confused with numerical artificial viscosity used to smear out shocks, instead the diffusion is implied by Boltzmann's equation to account for higher order dissipation.

The shock profiles of R13 can be compared to the results of the direct simulation Monte-Carlo-method (DSMC) of Bird (1998). For the DSMC results we use the shock structure code which is available from Bird's website. For the actual setup like interval length and upstream temperature the values of Pham-Van-Diep et al. (1991) have been adopted Note that the calculation of a single low Mach number shock structure by a standard DSMC program may take hours which is several orders of magnitude slower than the calculation by a continuum model. The computations are done for Maxwell molecules as interaction model.

We will compare the profiles of density and heat flux. The heat flux in a shock wave follows solely from the values of temperature and velocity after integration of the

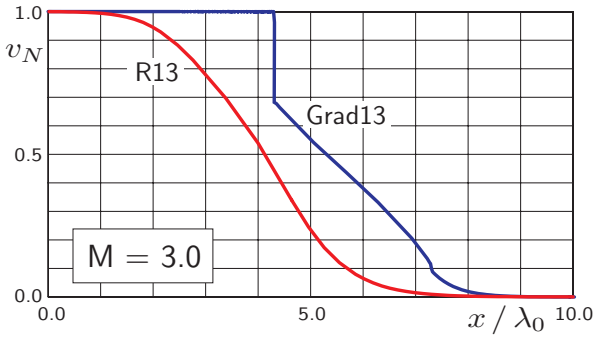

Figure 9: Comparison of a shock profile for velocity predicted from Grad's 13-moment-equations and R13 at Mach number $M = 3.0$. The subshocks in the Grad result are unphysical.

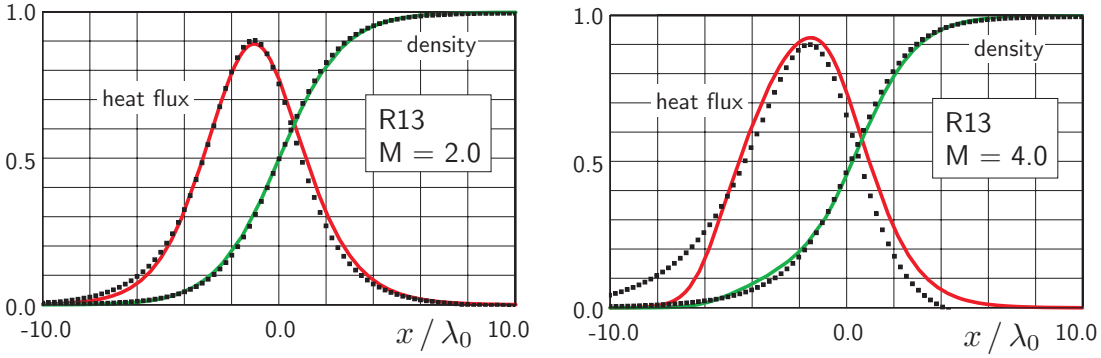

Figure 10: Shock profiles for normalized density and heat flux from R13 compared with DSMC results (dots).

conservation laws. Hence, its profile gives a combined impression of the quality of the temperature and velocity profile. The soliton-like shape of the heat flux helps also to give a better view of the quality of the structure. Since it is a higher moment the heat flux is more difficult to match than the stress or temperature. We suppress the profiles of velocity, temperature and stress. The density is normalized to give values between zero and unity for each Mach number. Similarly, the heat flux is normalized such that the DSMC result gives a maximal heat flux of +0.9.

In Fig. 10 the shock structures for the Mach numbers $M_0 = 2$ and $M_0 = 4$ calculated with the R13 are displayed together with the DSMC result. For the lower Mach number the density profile and the shape of the heat flux is captured very well by the R13 result. The deviations from the DSMC solutions become more pronounced for higher Mach numbers. In the plots for $M_0 = 4$ the R13 results starts to deviate from the DSMC solution in the upstream part. For higher Mach numbers the regularized 13-moment-equations deviates even more from the DSMC result and applicability of the theory is no longer given, if quantitative features are needed to be captured.

Accurate shock profiles for higher Mach numbers remain a strong challenge for moment equations and continuum model in general. The reason is strong bimodal distribution function inside the shock and a Knudsen number of essential unity. The thesis of Mc-

Donald (2010) demonstrated for a model system that moment models produce accurate results for strong shocks if a nonlinear closure is used and the collision integral does not introduce additional errors.

5.2 Multi-Dimensional Shock Simulation

This section is devoted to a specific flow situation in which a shock wave interacts with a density disturbance. The example is chosen to demonstrate the ability of the R13 equations for two-dimensional high-speed flows with shocks but no boundaries. The interaction of high speed flows with boundaries remains under investigation.

The scenario of the initial conditions is the following. The two-dimensional computational domain is given by $(x, y) \in [-2, 3] \times [-1, 1]$. A shock wave profile is situated with its density barycenter at $x = -1.0$ traveling in positive x-direction with Mach number $M_0 = 2.0$ into a flow field at rest with $(\rho, \theta, p) = (1, 1, 1)$. Around $(x, y) = (0.5, 0.0)$ a circular density cloud is placed with density distribution

$$\rho\,(x, y) = 1 + 1.5 \exp\left(-16\left(x^2 + y^2\right)\right) \tag{86}$$

and constant pressure. Due to constant pressure the interior of the bubble will be colder than the environment. The simulations will be based on dimensionless R13 equations for Maxwell molecules in which only the Knudsen number remains to be specified. We choose as an example $Kn = 0.1$, hence, the distance $\Delta x = 1$ which is roughly the extension of the density disturbance corresponds to 10 mean free paths of the reference state. The initial shock wave profile was computed in a preceding one-dimensional calculation and inserted into the 2D domain. More details of the computation and numerical method can be found in Torrilhon (2006).

For comparison the whole simulation is repeated using the Navier-Stokes-Fourier system. In that case also the shock profile was based on a preceding NSF calculation, since the shock profile differs for both models. At Knudsen numbers larger than 0.01 the solutions of the Navier-Stokes-Fourier model and the R13 equations start to deviate significantly. Due to the higher physical accuracy of the R13 system we expect its solution to be the physically more relevant one.

To give an impression of the distortion of the shock front due to the bubble Fig. 11 shows contour plots of temperature and heat flux amplitude various fields at time $t = 0.9$ in a section of the computational domain. The result shown is based on $Kn = 0.5$. At the time shown in the figure the front has fully passed through the cloud. The cloud is now placed behind the shock. The shock front is dented due to the interaction. A strong kink is also visible in the soliton shaped heat flux which interacts with the heat flux inside the bubble.

When comparing R13 and NSF, any difference must be related to the first order character of the constitutive relations of NSF which becomes most pronounced for larger Knudsen numbers. At time $t = 0.8$ the shock front is just about to exit the cloud. This situation shows the strongest non-equilibrium and correspondingly the strongest differences between the models. One-dimensional cuts for temperature and heat flux component q_x along $y = 0$ in the case $Kn = 0.1$ are shown in Fig. 12. The dashed lines in the temperature plot give a reference to the unperturbed fields of the shock front and density cloud, respectively. The solution of the NSF system is shown using thin lines.

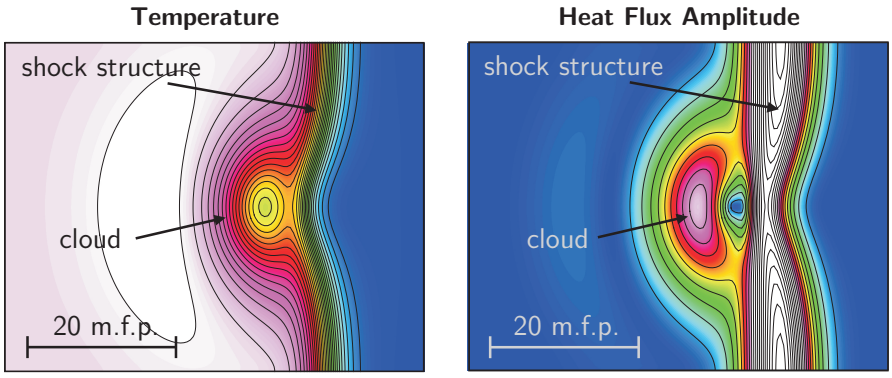

Figure 11: Interaction of a shock with a density disturbance (cloud) at $M = 2.0$ computed with R13.

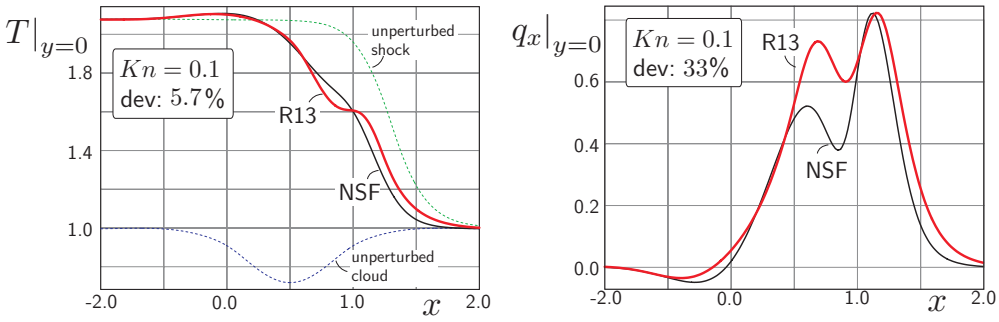

Figure 12: Comparison of the Shock-Cloud-Interaction with the result of Navier-Stokes-Fourier.

Generally speaking, the system of Navier-Stokes and Fourier introduce to much dissipation and shoulders like the temperature profile are washed out quickly in the NSF result. The maximal relative deviation between the models is included in each plot. The deficiency of Navier-Stokes-Fourier is manifested in more than 30% deviations in the heat flux.

We note that the differences originate purely from the lack of accurate high order non-equilibrium multi-scale modeling in the simple NSF system. In that sense the deviations are a bulk effect and can obviously not be influenced by boundary conditions as in slip models.

5.3 Hyperbolicity

If we ask for traveling wave solutions $\hat{W}(x - ct)$ of a quasi-linear system of partial differential equations in the form

$$\partial_t W + A(W)\, \partial_x W = 0 \tag{87}$$

we immediately find that the possible speeds of propagation c are eigenvalues of the flux matrix according to

$$\left(c\, I - A(\hat{W})\right) \hat{W} = 0 \tag{88}$$

where I is the identity matrix. The requirement of real-valued propagation speeds is a natural nonlinear extension of the linear idea of advection. Together with diagonalizability of the flux matrix, this is equivalent to hyperbolicity of the system.

When relaxation and dissipation is neglected from the system, that is, $m_{ijk} = \bar{R}_{ij} = 0$ and $\nu \to 0$ in Sec. 2.3, the R13 system has precisely the form of (87). This situation can be compared to the free-flight scenario, i.e., $Kn \to \infty$, when the homogeneous Boltzmann equation $\partial_t f + c_i \partial_i f = 0$ becomes valid. Obviously, a moment model with only a few moments is doomed to fail in a comparison to Boltzmann solutions since very general discontinous distribution functions may arise, see Au et al. (2001). Still, moment equations bear some significance in this situation in the sense that the possible propagation modes can be interpreted by particle packages with single nonlinear speed. However, the actual modes remain artificial because they depend solely on the choice and number of moments.

5.3.1 Speed of propagation

The homogeneous system of the form (87) for R13 coincides with the homogeneous system of Grad's 13-moment case. The two-dimensional equilibrium case of the speed of propagation is also sketched by Grad (1958). In two space dimensions the flux matrix $A(W)$ is 9×9 with entries

$$A = \begin{pmatrix}
v_x & \rho & 0 & 0 & 0 & 0 & 0 & 0 & 0 \\
0 & v_x & 0 & 0 & \frac{1}{\rho} & 0 & 0 & 0 & 0 \\
0 & 0 & v_x & 0 & 0 & 0 & \frac{1}{\rho} & 0 & 0 \\
0 & p + \frac{2}{3}p_x & \frac{2}{3}\sigma & v_x & 0 & 0 & 0 & \frac{2}{3} & 0 \\
0 & 3p_x & 0 & 0 & v_x & 0 & 0 & \frac{6}{5} & 0 \\
0 & p_x & 2\sigma & 0 & 0 & v_x & 0 & \frac{2}{5} & 0 \\
0 & 2\sigma & p_y & 0 & 0 & 0 & v_x & 0 & \frac{2}{5} \\
\frac{p(2p-7p_x)}{2\rho^2} & \frac{16}{5}q_x & 0 & \frac{7p_x-4p}{2\rho} & \frac{2p-p_x}{\rho} & 0 & -\frac{\sigma}{\rho} & v_x & 0 \\
-\frac{7p\sigma}{2\rho^2} & \frac{7}{5}q_y & \frac{7}{5}q_x & \frac{7\sigma}{2\rho} & -\frac{\sigma}{\rho} & 0 & \frac{2p-p_x}{\rho} & 0 & v_x
\end{pmatrix} \tag{89}$$

using the notation of Sec. 2.5. The propagation speeds are given by the eigenvalues of A which have the form

$$\lambda_j = v_x + c_j \left(\frac{p_x}{p}, \frac{p_y}{p}, \frac{\sigma}{p}, \frac{q_x}{p\sqrt{\theta}}, \frac{q_y}{p\sqrt{\theta}} \right) \sqrt{\theta} \qquad j = 1, 2, ...9 \tag{90}$$

but can not be derived explicitly in general. In "equilibrium", i.e., $\sigma = q_x = q_y = 0$ and $p_x = p_y = p$, the values of c_j are given in the form of multiple roots. They evaluate to be

$$\{c_j\}_{j=1,2...8} = \{0, 0, \pm 0.812, \pm 1.183, \pm 2.130\}\,. \tag{91}$$

Especially, the largest absolute value takes the form

$$\lambda^{(0)}_{\max} = |v_x| + 2.130\sqrt{\theta} = |v_x| + 1.65\sqrt{\gamma\,\theta}, \tag{92}$$

with adiabatic constant $\gamma = 5/3$, hence, the propagation speed is 1.65 times the adiabatic sound speed, a value already given by Grad (1949).

There exists some confusion about the relevance of the characteristic speeds (91), especially in comparison with the speeds of the Euler/NSF equations given by $v_x \pm \sqrt{\gamma\,\theta}$

and v_x for a monatomic gas. However, to some extent this comparison is misleading. Even though the speeds are evaluated for vanishing stress and heat flux, the situation still represents collisionless flight of particle which can hardly be compared to collision-dominated equilibrium. In the R13 system the sound modes in equilibrium are the result of the interaction between the hyperbolic modes of the homogeneous system and the dissipation and relaxation as shown in Torrilhon (2000).

We investigate the value of the fastest propagation speed for different values of directional temperatures, shear stress and heat flux. In non-equilibrium the distribution function deviates from the isotropic Maxwellian. Different directional temperatures introduce an ellipsoidal shape and the heat flux specifies a preferred direction. The propagation speed of the homogeneous system (91) reflects this behavior. Fig. 13 gives some snapshots of the two-dimensional signal speeds arising from different non-equilibrium situations. Note, that the speed in a certain direction $\mathbf{n}$ can be calculated from the one-dimensional result (90) by rotating the values of heat flux and pressure tensor into the required direction. The plots in the figure are Friedrichs-diagrams in which the fastest signal mode is displayed as parametric curve $c_{\max}(\mathbf{n})\,\mathbf{n}$. The line represents a wave front after one time unit started as point from the origin. Additionally, in each plot the shape of the stress tensor is sketched as its action to a circular volume. The direction of the heat flux is shown as arrow. The directional temperatures $\hat{\theta}_1$ and $\hat{\theta}_2$ are calculated in the directions of the eigenvectors of the stress tensor.

The upper left pictures shows the isotropic equilibrium situation, the picture right to it the presence of stress with no heat flux and the picture below the presence of a heat flux with no stress. The remaining three plots display the interaction between stress and heat flux in different directions. The figure demonstrates the ability of the homogeneous system to approximate the principal shape of the underlying velocity distribution function.

5.3.2 Loss of Hyperbolicity

It is known that the expression (90) will not yield real values for all non-equilibrium states, see Müller and Ruggeri (1998) or Torrilhon (2000). Indeed, only in some vicinity of equilibrium this can be assured. This means the homogeneous system is hyperbolic only in a specific domain of hyperbolicity. The region of hyperbolicity can be displayed in the plane opened by the dimensionless normal stress σ/p and the dimensionless heat flux $q_x/(\rho\theta^{3/2})$. Because the pressure tensor p_{ij} is positive definite the normal stress can only take values $\sigma/p \in [-1, 2]$. Fig. 14 shows this projected phase space with the region of hyperbolicity for Grad's 13-moment equations. The dot in the middle marks equilibrium $\sigma = 0$ and $q_x = 0$. The contours give the value of the fastest speed of propagation.

At some points in the phase space the maximal real eigenvalue of the flux matrix will coincide with another eigenvalue and produce a complex conjugated pair. At these points a real-valued maximal speed of propagation simply ceases to exist. The system looses hyperbolicity and also physicality due to complex-valued propagation speeds. As depicted in Fig. 14 hyperbolicity is given only for moderate heat fluxes and large enough stress values. For large values of the heat flux and for very small values of σ/p hyperbolicity is lost. This loss is a nonlinear phenomenon. The linearized equations consider deviations close to equilibrium and remain hyperbolic for arbitrary values of these deviations. Furthermore, linear wave are entirely stable in the R13 system both with and without dissipation.

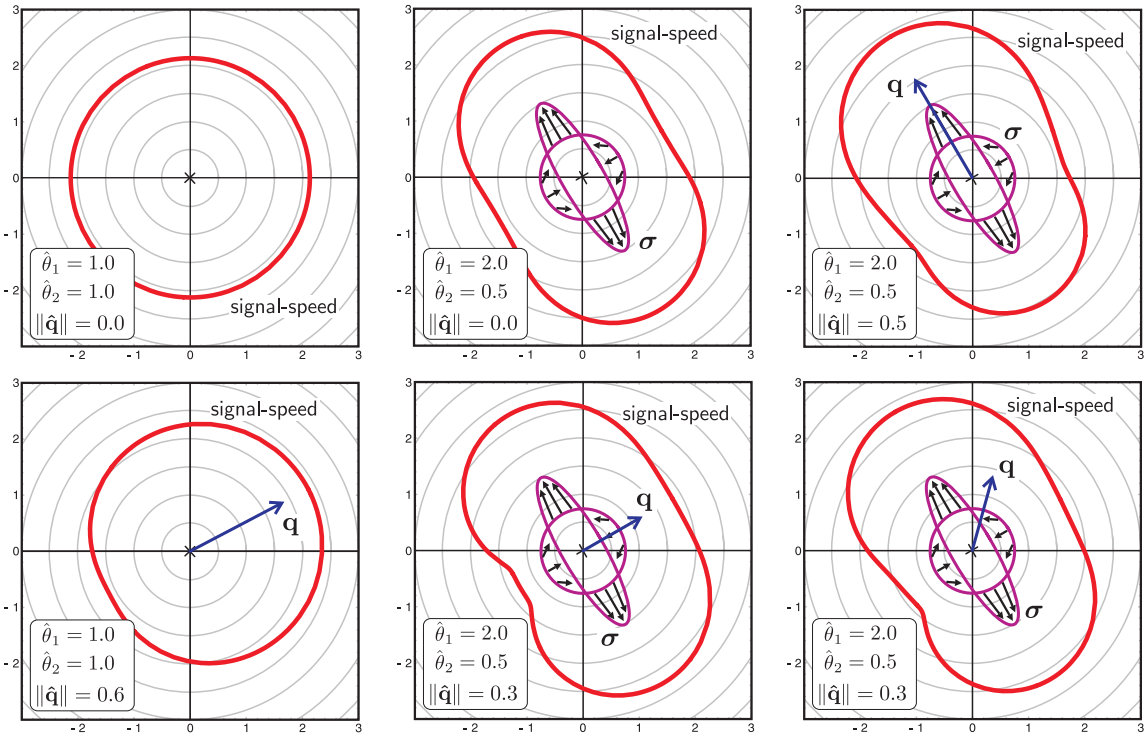

Figure 13: Two-dimensional maximal signal speed for the homogeneous Grad's 13-moment-system. Different non-equilibrium states distort the signal speed similar to the shape of a corresponding distribution function. The purple drawing indicate a sketch of the stress situation.

To demonstrate the influence of this lack of hyperbolicity we compute a shock tube problem with the homogeneous system (87), see also Torrilhon (2010a) and Torrilhon (2000) for details. For small density and pressure ratios of the initial conditions the solution stays within the hyperbolicity region. For a shock tube with equal density and pressure ratio of 6.5 the result is shown in the phase space of Fig. 14 as a polygon parameterized by the spatial variable. This solution leaves the region of hyperbolicity. Complex eigenvalues lead to strong oscillations which grow and lead to a break down of the computation due to negative densities. This behavior severely limits the application range of Grad's equations. It can not be improved by considering more moments Au et al. (2001), Brini (2001). The precise mathematical reason for the failure remains unclear. Most likely, the fact that the distribution function used in the equations of Grad becomes negative causes trouble, see Struchtrup (2005b).

Loss of hyperbolicity is often brought forward as an objection against the usefulness of e.g., Grad's equations. However, there is an important issue that refutes this objection. Note, that the shock tube problem above is computed in the collisionless situation. As soon as relaxation and dissipation are added the non-equilibrium, that is, the values of stress and heat flux, are reduced and the solution gets back into the hyperbolicity domain. Hence, the loss occurs only at a very high level of non-equilibrium represented by large Knudsen numbers. At this level, the equations are not valid because of their derivation as model for moderate Knudsen numbers. This statement can be quantified. The analysis of

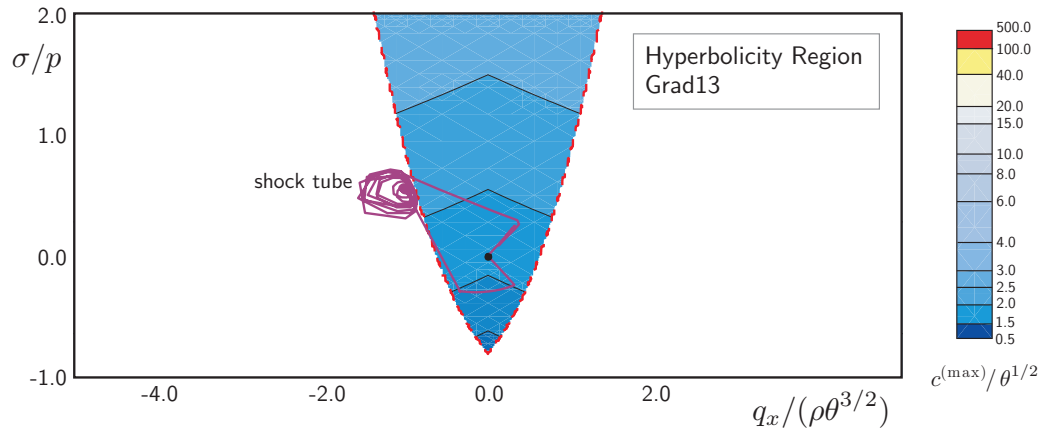

Figure 14: Hyperbolicity region of Grad's 13-moment-equations plotted in the projected physe space. The contours show the maximal signal speed. Additionally, the solution trajectory of initial layer for a shock tube simulation is drawn.

hyperbolicity shows that $p_{x,y}/p \lesssim 0.2$, and $\left\|q_i/(p\sqrt{\theta})\right\| \gtrsim 0.6$ leads to loss of hyperbolicity of the 13-moment-case, see Müller and Ruggeri (1998). To evaluate these conditions we consider the NSF relations (25) as approximation to σ_{ij} and q_i and deduct conditions on the relative change in velocity and temperature. We find $\Delta v/\sqrt{\theta} \lesssim 0.4\,\Delta x/\lambda$ and $\Delta\theta/\theta \lesssim 0.16\,\Delta x/\lambda$, i.e., relative change in velocity and temperature over a *single mean free path* is restricted to be below 40% and 16%, respectively. These conditions state a strong non-equilibrium at which the validity of the continuum model is not assured anymore. In any reasonable simulation based on the 13-moment-equation such a non-equilibrium should be avoided.

However, due to initial layers occasional violations of hyperbolicity can not be entirely ruled out in a numerical simulation. Experience shows that these violations due to occasional high non-equilibrium are usually quickly cured by damping and smoothing effects in the system. However, a numerical method should be robust enough to handle such a violation. Numerical evaluation of the eigenvalue shows that, even though some values turn complex, there will always be a direction with a fastest speed that is real.

5.3.3 Pearson Closure

Grad's 13 moment equation is the underlying model of the R13 system. When Grad considered moment equations in Grad (1949), Grad (1958) he solved the closure problem by assuming the general expression

$$f^{(\mathrm{Grad})}\left(\mathbf{x},t,\mathbf{c};\rho,\mathbf{v},\theta\right) = f_M\left(\mathbf{c};\,\rho,\mathbf{v},\theta\right)\left(1+\sum_{\alpha=1}^{N}\lambda_\alpha\left(\mathbf{x},t\right)\mathbf{c}_\alpha\right) \tag{93}$$

as model for the distribution function based on the Maxwellian distribution. Here, λ_α are parameters of the distribution function with multi-index α, such that $\mathbf{c}_\alpha = c_{i_1}\cdots c_{i_{|\alpha|}}$ to simplify the presentation. The Maxwellian in (93) depends on the local values of density, velocity and temperature which serve as additional parameters. For $N = 13$ the parameters of this distribution are linked to the 13 fields density, velocity, temperature, stress

and heat flux. After fixing the parameters all remaining higher moments for fluxes in the equations can be computed. The ansatz (93) represents a partial sum of a Hermite series for the distribution function written in monomials $\mathbf{c}_\alpha$. From a functional analytical point of view we assume that for smooth f this partial sum yields a reasonable approximation. With this interpretation Grad's distribution function is not restricted to be close to equilibrium. Still, for λ_α small in some sense (93) can be viewed as perturbation of a Maxwellian.

In general, in the theory of moment equations the closure is obtained from a model for the distribution function. A model of the distribution function has the form

$$f(\mathbf{x}, t, \mathbf{c}) = f^{(\text{model})}\left(\mathbf{c};\, \{\lambda_\alpha(\mathbf{x}, t)\}_{|\alpha|=1,2,\dots N}\right) \tag{94}$$

such that f depends on space and time through parameters λ_α. The number of parameters N represents the complexity of the model. We assume that the parameters can be computed from the first N moments after inserting $f^{(\text{model})}$ into the definition of the moments in Sec. 2.1 such that we have a one-to-one relation between parameters and moments. At this point the closure problem is solved because any higher moment can be computed.

Obviously, the Grad distribution (93) is not the only possibility for a model of a distribution function. Note, that only in equilibrium the shape of the distribution is fixed to be a Maxwellian. In general non-equilibrium the shape of the distribution is not known. Certainly, Grad's choice is problematic as it exhibit negative values in its tail for non-vanishing heat flux. This could also be the reason for the loss of hyperbolicity of the moment equations.

To tackle the problem of hyperbolicity a Pearson-Type-IV distribution was investigated in Torrilhon (2010a). This distribution is given by

$$f^{(\text{P3})}(\mathbf{c}\,; \lambda, \mathbf{A}, m, \nu, \mathbf{n}) = \frac{1}{\det(\mathbf{A})\, K} \frac{\exp\left(-\nu \arctan\left(\mathbf{n}^T \mathbf{A}^{-1}(\mathbf{c}-\lambda)\right)\right)}{\left(1 + (\mathbf{c}-\lambda)^T \mathbf{A}^{-2}(\mathbf{c}-\lambda)\right)^m} \tag{95}$$

with a shift vector $\lambda \in \mathbb{R}^3$, a positive-definite scale tensor $\mathbf{A} \in \mathbb{R}^{3\times 3}$, a skewness amplitude $\nu \in \mathbb{R}$ and skewness direction $\mathbf{n} \in S^2$ as well as a real-valued shape parameter $m > 0$. In this way the distribution is described by 14 real parameters. Additionally, a normalization constant K occurs in (95). It can be demonstrated that three-dimensional integrals of the distribution factorize into integrals over 1D Pearson distributions which can be solved analytically. This property is key to the computation of moments of the Pearson distribution.

The Pearson distribution above has 14 parameters. In order to use it as closure for the 13-moment equations one parameter has to be slaved to the others. Details of the derivation of the closure are given in Torrilhon (2010a). The result is a strongly nonlinear closure for the moments m_{ijk} and R_{ij}, relating these moments to lower order moments. Interestingly, the Grad closure can be obtained from the new expressions when linearizing in non-equilibrium variables.

The final equations based on the Pearson distribution show an clearly extended region of hyperbolicity. Fig. 15 shows the projected phase space as discussed above with the same plot range as in Fig. 14. Similarly, the contours represent the value of the fastest speed of propagation. Also, the contour spacing is identical in both figures for better

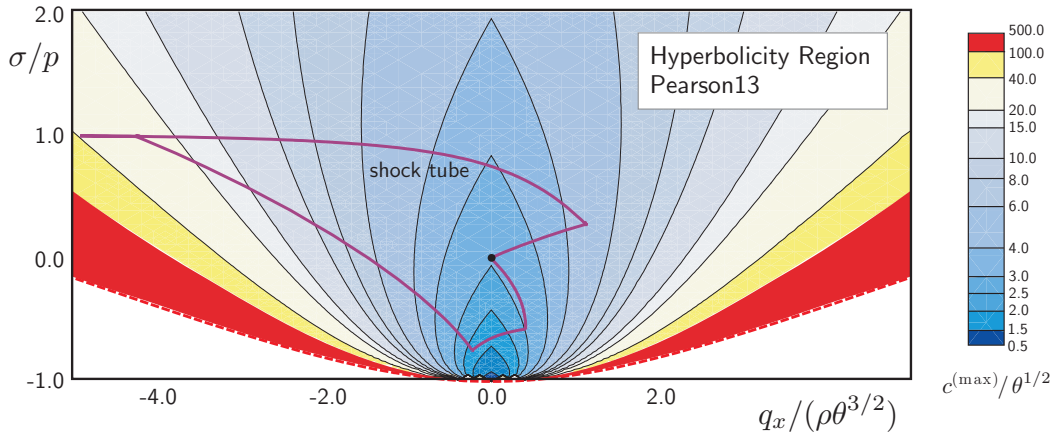

Figure 15: Hyperbolicity region of Pearson's 13-moment-equations plotted in the projected physe space. The contours show the maximal signal speed. For comparison the same color scaling as in Fig. 14 is used. Additionally, the solution trajectory of initial layer for a shock tube simulation is drawn.

comparison. Note, that still no global hyperbolicity is obtained. For small values of stress complex-valued eigenvalues occur, but the loss of hyperbolicity is robust in the following way. While in Grad's case a pair of eigenvalues join at some finite value and suddenly become a complex conjugated pair, the fastest eigenvalue in the Pearson case grows to infinity before becoming complex. In that sense ever faster speeds in the system indicate an upcoming loss of hyperbolicity.

Similar to Fig. 14 we show the result of a shock tube problem in the phase space in Fig. 15. It uses a large pressure and density ratio of 50 and exhibits strong non-equilibrium with large values of heat flux and extreme values of stress. Interestingly the solution stays away from the border of the hyperbolicity region.

So far, the Pearson closure has been developed only for the homogenous moment system without relaxation and regularization terms. A nonlinear closure combined with accurate relaxation might be able to produce high physical accuracy for instance for shock profiles as shown for a model system in McDonald (2010). The regularization would increase the accuracy further. However, since the regularization procedure is based on a Grad-type closure it has to be re-done based on the Pearson distribution.

6 Further Reading

This text serves as introduction to the fluid model given by the regularized 13-moment equations. It focuses on the presentation of the equations in various formulations and provides insights to fundamental linear and nonlinear solutions obtained in recent years. More details about the derivation of the system can be found in the text book by Struchtrup (2005b).

The range of results and applications for the R13 system is not complete. More examples, like a thermal version of the Knudsen paradox, can be found in the review by Torrilhon and Struchtrup (2008b). Taheri and Struchtrup (2010a) consider the flow

through cylindrical channels and nonlinear and linear effects in thermal creep flows have been investigated in Taheri and Struchtrup (2010b). More research on moment systems in general can be found in the special issues of *Continuum Mechanics and Thermodynamics* on the occasion of an international conference on moment methods, see Torrilhon (2009).

The regularization procedure can be used on any moment system to stabilize and increase physical accuracy. The 10-moment equations advocated by Levermore and Morokoff (1998) does not describe heat conduction. A regularization conducted by McDonald and Groth (2008) adds an anisotropic heat flux tensor based on the gradient of the temperature tensor. The R10 system is clearly superior to the simpler 10-moment equations, but it can not predict Knudsen layers or higher order bulk effects. Similarly, the R13 system has its limits on the accuracy of the predictions and larger moment systems will provide better results. Following this idea Gu and Emerson (2009) derived a regularized 26-moment system which shows better accuracy in channel flows and boundary layers, see Gu et al. (2010). Based on an advanced numerical approach Cai and Li (2010) have implemented regularized moment equations for an almost arbitrary number of moments. For large moments their method eventually becomes equivalent to an efficient solution strategy of the Boltzmann equation.

Related to the problem of global hyperbolicity is the questions of the existence of an entropy law for the R13 system. In the linear case as presented in Sec. 4.2 an entropy law with positive definite production is presented in Struchtrup and Torrilhon (2007). For the nonlinear equations based on Grad's closure an entropy remains unknown and the mathematical theory of the maximum entropy closure as in Levermore (1996) is not applicable. Presently, there seem to exist two approaches to this problem. One approach investigates how the maximum entropy closure can be used to produce practical equations. After initial work by Brown (1999) this approach has recently gained more perspective through McDonald (2010). The other approach to the question of entropy is of phenomenological nature. The equations of Grad or R13 could be altered in a nonlinear way such that an entropy law becomes admissible. Öttinger (2010) suggests an interesting change of variables but unfortunately his equations are not useful as shown by Struchtrup and Torrilhon (2010).

Finally, it is always an interesting question how moment equations could be coupled in a hybrid simulation with gas dynamics based on Navier-Stokes-Fourier and a direct solver of Boltzmann or DSMC, like in Roveda et al. (1998) or Sun et al. (2004). Most important in such an approach is the knowledge when to switch between the different models. The R13 theory provides natural switching criteria as presented in Lockerby et al. (2009). However, this has not yet be employed in full simulations.

References

Agarwal, R. K., Yun, K. Y., and Balakrishnan, R. (2001). Beyond navier-stokes: Burnett equations for flows in the continuum-transition regime. *Phys. Fluids*, 13:3061–3085. Erratum: Phys. Fluids 14, (2002), p.1818.

Alsmeyer, H. (1976). Density profiles in argon and nitrogen shock waves measured by the absorbtion of an electron beam. *J. Fluid Mech.*, 74(3):497.

Aoki, K. and Sone, Y. (1987). Temperature field induced around a sphere in a uniform flow of a rarefied gas. *Phys. Fluids*, 30(7):2286–2288.

Au, J. D. (2001). *Lösung nichtlinearer Probleme in der Erweiterten Thermodynamik*. PhD thesis, Technical University Berlin.

Au, J. D., Torrilhon, M., and Weiss, W. (2001). The shock tube study in extended thermodynamics. *Phys. Fluids*, 13(7):2423–2432.

Bailey, C. L., Barber, R. W., Emerson, D. R., Lockerby, D. A., and Reese, J. M. (2005). A critical review of the drag force on a sphere in the transition flow regime. In Capitelli, M., editor, *24th Intl. Symp. on Rarefied Gas Dynamics*. AIP-Proceedings.

Barber, R. W. and Emerson, D. R. (2003). Numerical simulation of low Reynolds number slip flow past a confined microsphere. In Ketsdever, A. D. and Muntz, E. P., editors, *23rd Intl. Symp. on Rarefied Gas Dynamics*. AIP-Proceedings.

Batchelor, G. K. (2000). *An Introduction to Fluid Dynamics*. Cambridge University Press.

Bird, G. A. (1998). *Molecular Gas Dynamics and the Direct Simulation of Gas Flows*. Oxford University Press, 2nd edition.

Bobylev, A. (1982). The Chapman-Enskog and Grad methods for solving the Boltzmann equation. *Sov. Phys. Dokl.*, 27:29–31.

Boltzmann, L. (1872). Weitere Studien über das Wärmegleichgewicht unter Gasmolekülen. *Wiener Berichte*, 66:275–370.

Brini, F. (2001). Hyperbolicity region in extended thermodynamics with 14 moments. *Cont. Mech. Thermodyn.*, 13(1):1.

Brown, S. (1999). *Approximate Riemann Solvers for Moment Models of Dilute Gases*. PhD thesis, University of Michigan Ann Arbor.

Cai, Z. and Li, R. (2010). Numerical regularized moment method of arbitrary order for boltzmann-bgk equation. *SIAM J. Sci. Comput.*, 32(5):2875–2907.

Candler, G. V., Nijhawan, S., Bose, D., and Boyd, I. D. (1994). A multiple translational temperature gas dynamics model. *Phys. Fluids*, 6(11):3776–3786.

Cercignani, C. (1988). *The Boltzmann Equation and its Applications*. Applied Mathematical Sciences. Springer, New York.

Cercignani, C. (2000). *Rarefied Gas Dynamics: From Basic Concepts to Actual Calculations*. Texts in Applied Mathematics. Cambridge University Press.

Chapman, S. and Cowling, T. G. (1970). *The Mathematical Theory of Non-Uniform Gases*. Cambridge University Press.

Eu, B.-C. (1980). A modified moment method and irreversible themrodynamics. *J. Chemical Phys.*, 73(6):2958–2969.

Gilberg, D. and Paolucci, D. (1953). The structure of shock waves in the continuum theory of fluids. *J.Rat. Mech. Anal.*, 2.

Goldberg, R. (1954). *The Slow Flow of a Rarefied Gas Past a Spherical Obstacle*. PhD thesis, New York University.

Grad, H. (1949). On the kinetic theory of rarefied gases. *Comm. Pure Appl. Math.*, 2:331.

Grad, H. (1952). The profile of a steady plane shock wave. *Comm. Pure Appl. Math*, 5.

Grad, H. (1958). Principles of the kinetic theory of gases. In Flügge, S., editor, *Handbuch der Physik*, volume 12. Springer, Berlin.

Gu, X.-J. and Emerson, D. (2007). A computational strategy for the regularized 13 moment equations with enhanced wall-boundary conditions. *J. Comput. Phys.*, 225:263–283.

Gu, X.-J. and Emerson, D. (2009). A high-order moment approach for capturing non-equilibrium phenomena in the transition regime. *J. Fluid Mech.*, 636.

Gu, X.-J., Emerson, D., and Tang, G.-H. (2010). Analysis of the slip coefficient and defect velocity in the knudsen layer of a rarefied gas using the linearized moment equations. *Phys. Rev. E*, 81:016313.

Hadjiconstantinou, N. G. (2003). Comment on Cercignani's second-order slip coefficient. *Phys. Fluids*, 15:2352.

Hutchins, D. K., Harper, M. H., and Felder, R. L. (1995). Slip correction measurements for solid spherical particles by modulated dynamic light scattering. *Aerosol Sci. Tech.*, 22:202–218.

Jin, S., Pareschi, L., and Slemrod, M. (2002). A relaxation scheme for solving the Boltzmann equation based on the Chapman-Enskog expansion. *Acta Math. Appl. Sinica (Engl. Series)*, 18:37–61.

Jin, S. and Slemrod, M. (2001). Regularization of the burnett equations via relaxation. *J. Stat. Phys.*, 103(5-6):1009–1033.

Jou, D., Casas-Vazquez, J., and Lebon, G. (1996). *Extended Irreversible Thermodynamics*. Springer, Berlin, 2nd edition.

Junk, M. (1998). Domain of definition of levermore's five-moment system. *J. Stat. Phys.*, 93(5-6):1143–1167.

Junk, M. (2002). Maximum entropy moment systems and galilean invariance. *Cont. Mech. Thermodyn.*, 14:563–576.

Karlin, I. V., Gorban, A. N., Dukek, G., and Nonnenmacher, T. F. (1998). Dynamic correction to moment approximations. *Phys. Rev. E*, 57(2):1668–1672.

Karniadakis, G. E. and Beskok, A. (2001). *Micro Flows: Fundamentals and Simulation*. Springer, New York.

Kauf, P., Torrilhon, M., and Junk, M. (2010). Scale-induced closure for approximations of kinetic equations. *J. Stat. Phys.*, 41:848–888.

Knudsen, M. (1909). Die Gesetze der Molekularströmung und der inneren Reibungsströmung der Gase durch Röhren. *Ann. Phys.*, 333:75–130.

Lamb, H. (1993). *Hydrodynamics*. Dover Publications, 6th edition.

Levermore, C. D. (1996). Moment closure hierarchies for kinetic theories. *J. Stat. Phys.*, 83(5-6):1021–1065.

Levermore, C. D. and Morokoff, W. J. (1998). The Gaussian moment closure for gas dynamics. *SIAM J. Appl. Math.*, 59(1):72–96.

Lockerby, D. A. and Reese, J. M. (2003). High-resolution burnett simulations of micro couette flow and heat transfer. *J. Comput. Phys.*, 188(2):333–347.

Lockerby, D. A., Reese, J. M., and Struchtrup, H. (2009). Switching criteria for hybrid rarefied gas flow solvers. *Proc. Roy. Soc. A*, 465(2105):1581–1598.

Maxwell, J. C. (1879). On stresses in rarefied gases arising from inequalities of temperature. *Phil. Trans. Roy. Soc.(London)*, 170:231–256.

McDonald, J. G. (2010). *Extended Fluid-Dynamic Modelling for Numerical Solution of Micro-Scale Flows*. PhD thesis, University of Toronto.

McDonald, J. G. and Groth, C. P. T. (2008). Extended fluid-dynamic model for micron-scale flows based on gaussian moment closure. *46th AIAA Aerospace Sciences Meeting*, 691.

Müller, I., Reitebuch, D., and Weiss, W. (2003). Extended thermodynamics - consistent in order of magnitude. *Cont. Mech. Thermodyn.*, 15(2):411–425.

Müller, I. and Ruggeri, T. (1998). *Rational Extended Thermodynamics*, volume 37 of *Springer Tracts in Natural Philosophy*. Springer, 2nd edition.

Myong, R.-S. (2001). A computational method for Eu's generalized hydrodynamic equations of rarefied and microscale gasdynamics. *J. Comput. Phys.*, 168(1):47–72.

Öttinger, H. C. (2010). Thermodynamically admissible 13 moment equations from the Boltzmann equation. *Phys. Rev. Letters*, 104:120601.

Pham-Van-Diep, G. C., Erwin, D. A., and Muntz, E. P. (1991). Testing continuum descriptions of low-mach-number shock structures. *J. Fluid Mech.*, 232:403.

Roveda, R., Goldstein, D. B., and Varghese, P. L. (1998). Hybrid euler/particle approach for continuum/rarefied flow. *J. Spacecr. Rockets*, 35(3):258.

Ruggeri, T. (1993). Breakdown of shock wave structure solutions. *Phys. Rev. E*, 47.

Satofuka, N., Morinishi, K., and Oishi, T. (1993). Numerical solutions of the kinetic model equations for hypersonic fows. *Comput. Mech.*, 11(5/6):452–464.

Seeger, S. and Hoffmann, H. (2000). The comulant method in computational kinetic theory. *Cont. Mech. Therm.*, 12(6):403.

Sharipov, F. and Seleznev, V. (1998). Data on internal rarefied gas flows. *J. Phys. Chem. Ref. Data*, 27(3):657–706.

Sone, Y. (2002). *Kinetic Theory and Fluid Dynamics*. Birkhauser, Basel.

Struchtrup, H. (2002). Heat transfer in the transition regime: Solution of boundary value problems for Grad's moment equations via kinetic schemes. *Phys. Rev. E*, 65:041204.

Struchtrup, H. (2004). Stable transport equations for rarefied gases at high orders in the Knudsen number. *Phys. Fluids*, 16(11):3921–3934.

Struchtrup, H. (2005a). Derivation of 13 moment equations for rarefied gas flow to second order accuracy for arbitrary interaction potentials. *Multiscale Model. Simul.*, 3(1):221–243.

Struchtrup, H. (2005b). *Macroscopic Transport Equations for Rarefied Gas Flows*. Interaction of Mechanics and Mathematics. Springer, New York.

Struchtrup, H. and Torrilhon, M. (2003). Regularization of Grad's 13-moment-equations: Derivation and linear analysis. *Phys. Fluids*, 15(9):2668–2680.

Struchtrup, H. and Torrilhon, M. (2007). H-theorem, regularization, and boundary conditions for linearized 13 moment equations. *Phys. Rev. Letters*, 99:014502.

Struchtrup, H. and Torrilhon, M. (2008). High order effects in rarefied channel flows. *Phys. Rev. E*, 78:046301. Erratum: Phys. Rev. E 78, (2008), 069903E.

Struchtrup, H. and Torrilhon, M. (2010). Comment on 'Thermodynamically admissible 13 moment equations from the Boltzmann equation'. *Phys. Rev. Letters*, 105:128901.

Sun, Q., Boyd, I. D., and Candler, G. V. (2004). A hybrid continuum/particle approach for modeling subsonic, rarefied gas flows. *J. Comput. Phys.*, 194:256–277.

Suzuki, Y. and van Leer, B. (2005). Application of the 10-moment model to MEMS flows. *43rd AIAA Aerospace Sciences Meeting*, 2005-1398.

Taheri, P. and Struchtrup, H. (2010a). An extended macroscopic transport model for rarefied gas flows in long capillaries with circular cross section. *Phys. Fluids*, 22:112004.

Taheri, P. and Struchtrup, H. (2010b). Rarefaction effects in thermally-driven microflows. *Physica A*, 389:3069–3080.

Taheri, P., Torrilhon, M., and Struchtrup, H. (2009). Couette and poiseuille microflows: Analytical solutions for regularized 13-moment equations. *Phys. Fluids*, 21:017102.

Takata, S., Sone, Y., and Aoki, K. (1993). Numerical analysis of a uniform flow of a rarefied gas past a sphere on the basis of the boltzmann equation for hard-sphere molecules. *Phys. Fluids A*, 5(3):716–737.

Torrilhon, M. (2000). Characteristic waves and dissipation in the 13-moment-case. *Cont. Mech. Thermodyn.*, 12:289.

Torrilhon, M. (2006). Two-dimensional bulk microflow simulations based on regularized 13-moment-equations. *SIAM Multiscale Model. Simul.*, 5(3):695–728.

Torrilhon, M. (2009). Editorial: Special issue on moment methods in kinetic gas theory. *Continuum Mech. Thermodyn.*, 21:341–343.

Torrilhon, M. (2010a). Hyperbolic moment equations in kinetic gas theory based on multi-variate Pearson-iv-distributions. *Comm. Comput. Phys.*, 7(4):639–673.

Torrilhon, M. (2010b). Slow rarefied flow past a sphere: Analytical solutions based on moment equations. *Phys. Fluids*, 22:072001.

Torrilhon, M. and Struchtrup, H. (2004). Regularized 13-moment-equations: Shock structure calculations and comparison to burnett models. *J. Fluid Mech.*, 513:171–198.

Torrilhon, M. and Struchtrup, H. (2008a). Boundary conditions for regularized 13-moment-equations for micro-channel-flows. *J. Comput. Phys.*, 227(3):1982–2011.

Torrilhon, M. and Struchtrup, H. (2008b). Modeling micro-mass and -heat transfer for gases based on extended continuum models. *ASME J. Heat Transfer*, 131:033103.

Uribe, F. J., Velasco, R. M., and Garcia-Colin, L. S. (1998). Burnett description of strong shock waves. *Phys. Rev. Lett.*, 81:2044.

Vincenti, W. G. and Kruger, C. H. (1965). *Introduction to Physical Gas Dynamics*. Wiley, New York.

Weiss, W. (1995). Continuous shock structures in extended thermodynamics. *Phys. Rev. E*, 52.

Xu, K. (2001). A gas-kinetic BGK scheme for the Navier-Stokes equations and its connection with artificial dissipation and Godunov method. *J. Comput. Phys.*, 171:289–335.

Xu, K. (2002). Regularization of the Chapman-Enskog expansion and its description of shock structure. *Phys. Fluids (Letters)*, 14(4):L17–L20.

Xu, K. and Li, Z.-H. (2004). Microchannel flow in the slip regime: Gas-kinetic BGK-burnett solutions. *J. Fluid Mech.*, 513:87–110.

Zheng, Y., Garcia, A. L., and Alder, J. B. (2002). Comparison of kinetic theory and hydrodynamics for Poiseuille flow. *J. Stat. Phys.*, 109:495–505.

Zhong, X., MacCormack, R. W., and Chapman, D. R. (1993). Stabilization of the Burnett equations and applications to hypersonic flows. *AIAA Journal*, 31:1036.